RSC Pharmaceutics

ROYAL SOCIETY OF CHEMISTRY

PAPER

View Article Online
View Journal | View Issue

Cite this: *RSC Pharm.*, 2026, **3**, 778

Biogenic chitosan anchored Cu_2O/ZnO nanocomposite: unlocking synergy for drug delivery, antineoplastic action, and wound repair

Manojna R. Nayak,[a] Ravindra R. Kamble, *[a] Lokesh Bheemayya,[a] Vishwa B. Nadoni,[a] Amruta Patri,[a] Mallika Wali,[a] Arun K. Shettar,[b] Joy H. Hoskeri,[c] Rangappa S. Keri[d] and Ashok M. Sajjan[e]

The clinical efficacy of many chemotherapeutic agents is often limited by inefficient drug delivery, poor selectivity toward cancer cells, and insufficient support for tissue regeneration. To address these challenges, we report the green synthesis of a multifunctional chitosan-anchored Cu_2O/ZnO nanocomposite (CS-Cu_2O/ZnO NC) using water calyx fluid (WCF) extracted from *Spathodea campanulata* flower buds as a natural reducing and stabilizing agent. Structural and physicochemical characterization using X-ray diffraction confirmed the crystalline phases of Cu_2O and ZnO, while UV-Vis spectroscopy showed characteristic absorption in the 270–320 nm region indicating nanoparticle formation. FTIR analysis verified the successful integration of chitosan and phytochemical functional groups with metal oxides. Transmission electron microscopy revealed quasi-spherical nanoparticles uniformly distributed within the polymer matrix with an average particle size of 20–40 nm, whereas dynamic light scattering showed a hydrodynamic diameter of ~89.3 nm with a zeta potential of −29.4 mV, confirming good colloidal stability. The nanocomposite was employed as a carrier for cisplatin and exhibited high drug loading efficiency with a biphasic release profile, achieving 94.88% cumulative drug release over 72 h. *In vitro* cytotoxicity studies demonstrated enhanced anticancer activity against A375 skin cancer cells (IC_{50} = 29.84 μg mL^{-1}) with comparatively lower toxicity toward L929 fibroblast cells. Furthermore, scratch wound healing assays revealed significant fibroblast cell migration and accelerated wound closure within 24 h, highlighting the regenerative potential of the nanocomposite. Overall, the developed green-synthesized CS-Cu_2O/ZnO nanocomposite represents a sustainable multifunctional platform for controlled drug delivery, cancer therapy, and wound healing applications.

Received 22nd December 2025,
Accepted 6th April 2026

DOI: 10.1039/d5pm00392j

rsc.li/RSCPharma

1. Introduction

Nanotechnology has ushered in a new era of medical innovation, offering unique solutions to longstanding healthcare challenges.[1,2] Nanotechnology has emerged as a transformative paradigm in the field of biomedical sciences, enabling the development of highly functional nanostructured materials for diagnostic, therapeutic, and regenerative applications. Among the diverse array of nanomaterials, metal oxide nanoparticles have gained considerable attention due to their distinctive physicochemical properties, including high surface area-to-volume ratios, tunable surface functionalities, and inherent biological activity.[3,4] In particular, copper oxide (Cu_2O) and zinc oxide (ZnO) nanoparticles have been extensively investigated for their promising antibacterial, antioxidant, and anticancer properties, making them ideal candidates for integration into drug delivery systems.[5–7] However, the intrinsic cytotoxicity and agglomeration tendencies of metal oxides in biological media necessitate the development of biocompatible platforms that can stabilize these nanoparticles and enhance their therapeutic efficacy.

Chitosan, a naturally occurring polysaccharide derived *via* the deacetylation of chitin, provides a highly versatile biopolymeric scaffold for the fabrication of nanocarriers owing to its exceptional biocompatibility, intrinsic biodegradability, and pronounced mucoadhesive characteristics.[8–10] Beyond these attributes, it demonstrates inherent antimicrobial activity and remarkable film-forming capacity, while its cationic nature enables strong electrostatic interactions with anionic drugs

[a]*Department of Studies in Chemistry, Karnatak University, Dharwad, 580003, India. E-mail: ravichem@kud.ac.in*
[b]*Division of Preclinical Research and Drug Development, Cytxon Biosolutions Pvt Ltd, Hubli, 580031, India*
[c]*Department of Bioinformatics and Biotechnology, Karnataka State Akkamahadevi Women's University, Vijayapura, 586108, India*
[d]*Centre for Nano and Material Science, Jain University, Bengaluru 562112, India*
[e]*Department of Chemistry, KLE Technological University, Hubballi, 580031, India*

and biomolecules.[11] Crucially, the abundance of reactive amino and hydroxyl functionalities within its backbone permits facile chemical functionalization and covalent cross-linking with inorganic nanomaterials, thereby enhancing structural integrity, improving physicochemical stability, and enabling finely regulated drug release kinetics.[12] The strategic incorporation of Cu_2O and ZnO nanoparticles within the chitosan framework culminates in the development of a multifunctional nanocomposite, synergistically uniting mechanical robustness, bioactivity, and advanced drug delivery capability. Compared with single metal oxide nanoparticles such as ZnO, CuO, or TiO_2, the Cu_2O/ZnO hybrid system offers synergistic physicochemical and biological properties. ZnO provides excellent biocompatibility and antimicrobial activity, whereas Cu_2O contributes strong redox activity and reactive oxygen species generation that enhance anticancer performance. The integration of both metal oxides within a single nanocomposite improves stability, catalytic activity, and therapeutic performance compared with individual nanoparticles.

Conventional nanoparticle fabrication strategies often necessitate the use of hazardous reducing agents, energy-demanding conditions, and ecologically harmful solvents, thereby engendering profound risks to both human well-being and environmental sustainability. Conversely, green synthetic methodologies offer a viable, eco-conscious paradigm by harnessing phytochemical-rich plant extracts that act dually as reducing and stabilizing agents.[13,14] This phytogenic route exploits an array of naturally occurring bioactive constituents such as flavonoids, alkaloids, polyphenols, and tannins not only to facilitate the reduction of metal ions into nanoscale entities but also to endow them with inherent biological functionalities.[15] Typically executed under benign, ambient conditions, these methods circumvent the necessity for toxic reagents or elevated thermal inputs, thereby epitomizing the foundational principles of green chemistry. Within the spectrum of botanical species investigated for sustainable nanofabrication, *Spathodea campanulata* (African tulip tree) emerges as particularly noteworthy owing to its rapid proliferation, ornamental prominence, and diverse pharmacological repertoire (Fig. S1).[16–19] Its floral buds are enriched with secondary metabolites exhibiting pronounced antioxidant and antimicrobial potential, rendering them highly advantageous for eco-benign nanoparticle synthesis.[20,21] In the present investigation, the water calyx fluid (WCF) of *Spathodea campanulata* was exploited as a natural bioreductant and stabilizing matrix for the green fabrication of a chitosan-anchored Cu_2O/ZnO nanocomposite (CS-Cu_2O/ZnO NC). This integrative approach not only mitigates the ecological footprint of the synthesis but also augments the physicochemical robustness, biofunctionality, and biomedical compatibility of the engineered nanostructure.

Table 1 summarizes commonly investigated metal oxide nanoparticles and their hybrid systems used for biomedical and catalytic applications. Although single metal oxides such as ZnO, TiO_2, Ag, and Cu exhibit strong antimicrobial and catalytic properties, they often suffer from limitations including rapid electron–hole recombination, restricted visible-light activity, high cost, or potential cytotoxicity. Hybrid nanocomposites such as ZnO/TiO_2 and ZnO/CuO have been devel-

Table 1 Comparative analysis of commonly reported metal oxide nanoparticles and nanocomposites[22–28]

Nanomaterial	Key characteristics	Advantages	Limitations	Representative applications
ZnO nanoparticles	Wide band gap semiconductor (~3.3 eV), high surface area, strong ROS generation	Good antibacterial and anticancer properties, cost-effective and relatively biocompatible	Rapid electron–hole recombination and limited visible-light absorption	Drug delivery, antimicrobial coatings, photocatalysis
TiO_2 nanoparticles	Chemically stable semiconductor with strong photocatalytic properties	High chemical stability and photocatalytic efficiency	Mainly active under UV light; limited visible light utilization	Environmental remediation, antibacterial coatings
Ag nanoparticles	Noble metal nanoparticles with strong antimicrobial ion release	Highly effective antibacterial and anticancer activity	High cost and potential cytotoxicity at higher concentrations	Wound dressings, antimicrobial coatings
Cu nanoparticles	Excellent catalytic and electrical properties	Low cost and strong antimicrobial activity	Easily oxidized; may cause cytotoxicity at higher doses	Catalysis, antibacterial materials
ZnO/TiO_2 nanocomposite	Binary semiconductor heterostructure	Improved charge separation and enhanced photocatalytic activity	Limited biological compatibility without surface modification	Photocatalysis, environmental remediation
CuO/TiO_2 nanocomposite	p–n heterojunction system	Enhanced photocatalytic and antibacterial activity due to synergistic interactions	Possible copper ion toxicity and stability issues	Antibacterial materials, catalytic systems
ZnO/CuO nanocomposite	Hybrid heterostructure improving visible light absorption	Reduced band gap and improved antimicrobial and photocatalytic performance	Potential instability and ion release issues	Environmental remediation and antibacterial applications
Cu_2O/ZnO nanocomposite (this work)	p–n heterojunction integrated with chitosan matrix *via* green synthesis	Enhanced ROS generation, improved drug loading and sustained release, increased antimicrobial and anticancer efficiency with improved biocompatibility	Requires controlled synthesis conditions to maintain stability and particle size	Drug delivery, anticancer therapy, wound healing applications

oped to overcome these drawbacks by improving charge separation and enhancing catalytic performance. In this context, the Cu_2O/ZnO nanocomposite developed in the present study, synthesized *via* a green route using *Spathodea campanulata* bud extract and stabilized with chitosan, offers additional advantages including improved biocompatibility, efficient drug loading, sustained release behavior, and enhanced biological activity, making it a promising multifunctional nanoplatform for biomedical applications.

To evaluate the prospective biomedical utility of the fabricated nanocomposite, cisplatin a platinum-based chemotherapeutic widely employed in oncology was selected as the model therapeutic for encapsulation. Despite its potent efficacy against a broad spectrum of malignancies, the clinical translation of cisplatin is profoundly constrained by its rapid systemic clearance and severe dose-limiting toxicities, including nephrotoxicity, ototoxicity, and myelosuppression.[29–31] The incorporation of cisplatin into a biopolymer-stabilized nanocarrier is envisaged to surmount these challenges by enhancing its aqueous solubility, facilitating tumor-targeted delivery, and maintaining sustained therapeutic concentrations, thereby reducing dosing frequency and minimizing systemic adverse effects.[32,33]

Drug delivery systems (DDS) represent engineered platforms meticulously designed to convey therapeutic agents to targeted biological sites with spatial precision and temporal control.[27–30] The advent of nanotechnology-enabled DDSs has markedly transformed the pharmacokinetic and pharmacodynamic profiles of conventional therapeutics, thereby amplifying their clinical efficacy and safety margins.[33–35] Furthermore, the incorporation of metal oxide moieties such as Cu_2O and ZnO not only augments the structural and functional attributes of the nanocarrier but also confers intrinsic therapeutic potential through reactive oxygen species (ROS) generation and selective cytotoxicity, thereby providing synergistic advantages for oncological interventions.[36,37]

Controlled drug release is a critical feature of modern DDSs, aimed at maintaining effective therapeutic drug levels over prolonged periods while minimizing side effects.[38,39] In chitosan-based nanocomposites, drug release mechanisms are governed by polymer swelling, erosion, and pH-sensitive degradation.[40–42] The presence of Cu_2O and ZnO nanoparticles contributes to the formation of a crosslinked matrix that can modulate drug diffusion. Furthermore, the acidic microenvironment of tumor tissues facilitates chitosan protonation, enhancing matrix swelling and promoting localized drug release.[43,44] Among these, chitosan-based nanocarriers have garnered particular prominence due to their intrinsic cationic character, which facilitates electrostatic interactions with negatively charged cellular membranes, promotes the transient opening of tight epithelial junctions, and consequently enhances intracellular uptake while prolonging drug retention at the site of action. In the present study, the synthesized CS-Cu_2O/ZnO NC exhibited a biphasic release profile, characterized by an initial burst followed by a sustained release over 72 hours.[45,46] This behavior is particularly advantageous in cancer therapy, where maintaining cytotoxic drug levels at the tumor site is essential for maximizing therapeutic efficacy while sparing healthy tissue.[47,48]

Furthermore, the exploration of wound healing applications offers an additional dimension to the biomedical relevance of such nanocomposites.[49] Wound repair is a highly regulated biological process involving coordinated cell migration, proliferation, and matrix remodeling.[50–52] Chitosan, with its intrinsic hemostatic, antimicrobial, and tissue-regenerative properties, has been widely studied in wound care formulations. When combined with bioactive metal oxides like Cu_2O and ZnO, the composite system may facilitate a supportive environment for cellular regeneration and tissue remodeling.[53–58] The evaluation of cell migration behavior *in vitro* serves as an important indicator of a material's regenerative potential.[59–62] Therefore, investigating the wound healing capacity of the synthesized chitosan-Cu_2O/ZnO nanocomposite provides valuable insight into its dual functionality not only as a drug delivery vehicle but also as a candidate material for use in skin repair and tissue engineering.

In summary, this study reports the green synthesis of a multifunctional chitosan-anchored Cu_2O/ZnO nanocomposite (CS-Cu_2O/ZnO NC) using WCF of *Spathodea campanulate* flower bud and its application as a targeted cisplatin delivery platform. The synthesized nanocomposite was thoroughly characterized by various analytical techniques to confirm its structural integrity, surface morphology, and physicochemical properties. The drug loading capacity, release kinetics, and biological efficacy were evaluated through *in vitro* cytotoxicity and wound healing assays. The findings highlight the potential of this green-engineered nanocomposite as a sustainable and effective drug delivery vehicle for cancer therapy and regenerative medicine.

2. Methods and methodology

2.1. Materials

Copper sulfate pentahydrate ($CuSO_4{\cdot}5H_2O$, ≥99% purity), zinc acetate dihydrate ($Zn(CH_3COO)_2{\cdot}2H_2O$, ≥99% purity), chitosan (medium to high molecular weight, 310–375 kDa), glacial acetic acid, and cisplatin were purchased from Sigma-Aldrich (India) and used without further purification. Fresh floral buds of *Spathodea campanulate* (Voucher No. KUD-BOT-SC-2025-017) were collected locally and authenticated by a qualified botanist (Fig. S2). All reagents used were of analytical grade, and deionized water was used throughout the experiments.

2.2. Preparation of *Spathodea campanulata* water calyx fluid (WCF)

Fresh floral buds of *Spathodea campanulata* were collected and thoroughly rinsed with deionized water to remove surface impurities. The buds were gently pierced using a sterile syringe to extract the internal liquid exudate, which is rich in phytochemicals. The collected liquid was filtered through Whatman No. 1 filter paper to remove particulate matter and used immediately for the nanoparticle synthesis. This freshly extracted water calyx fluid (WCF) served as a natural reducing

as well as stabilizing agent in this green synthesis of the nanocomposite (Fig. S3).

2.3. Green synthesis of chitosan-anchored Cu_2O/ZnO nanocomposite

The chitosan-anchored Cu_2O/ZnO nanocomposite (CS-Cu_2O/ZnO NC) was synthesized *via* a green approach using WCF of *Spathodea campanulata* flower bud as a bioreductant and stabilizing agent. Equimolar aqueous solutions of copper sulfate pentahydrate (0.1 M, 100 mL) and zinc acetate dihydrate (0.10 M, 100 mL) were prepared separately. These solutions were mixed in a 1 : 1 volume ratio under constant magnetic stirring at room temperature. A 2% (w/v) chitosan solution (100 mL), prepared by dissolving chitosan in 1% (v/v) glacial acetic acid, was then introduced slowly into the reaction medium. The presence of chitosan ensured stabilization and surface functionalization of the forming nanoparticles. Subsequently, freshly extracted WCF *Spathodea campanulata* (50 mL) collected directly using a sterile syringe was added dropwise to the metal ion solution. The reaction mixture was stirred continuously to facilitate reduction and nucleation. The reaction was allowed to proceed under ambient conditions for 24 hours. A visible color change into dark brown indicated the successful formation of the nanocomposite. The resulting precipitate was separated by centrifugation at 10 000 rpm for 10 minutes, washed thoroughly with deionized water and ethanol to remove unbound phytochemicals and residual ions, and subsequently dried in a hot air oven at 60 °C. The dried powder was collected and stored for further characterization and application (Scheme 1).

2.4. Characterization techniques

The physicochemical properties of the synthesized CS-Cu_2O/ZnO NC were thoroughly investigated using a range of analytical techniques. The crystalline structure and phase purity of the nanocomposite were determined using X-ray diffraction (XRD) analysis, performed on a Bruker D8 Advance diffractometer (Bruker AXS GmbH, Germany) equipped with Cu-Kα radiation (λ = 1.5406 Å) operated at 40 kV and 40 mA. The optical absorption characteristics and confirmation of nanoparticle formation were assessed using UV-visible spectroscopy (Shimadzu UV-2600, Japan) in the wavelength range of 200–800 nm. Fourier-transform infrared spectroscopy (FTIR) was conducted using a PerkinElmer Spectrum Two FTIR spectrometer (USA) in the range of 4000–400 cm^{-1} to identify surface functional groups and confirm the interaction between chitosan, metal oxides, and phytochemicals from the plant extract. Morphological analysis and particle size estimation were carried out using transmission electron microscopy (TEM; JEOL JEM-2100, Japan) operating at 200 kV, and scanning electron microscopy (SEM; ZEISS EVO 18, Germany). Energy Dispersive X-ray Spectroscopy (EDX), integrated with the SEM system, was utilized to confirm elemental composition and to map the spatial distribution of copper, zinc, oxygen, and other trace elements within the nanocomposite. Atomic force microscopy (AFM) was employed to evaluate surface topography and roughness using a Bruker Dimension Icon system (USA) operating in tapping mode. The colloidal stability and surface charge of the nanocomposite were assessed *via* zeta potential analysis using Horiba Scientific Nano Partica SZ-100 (Japan), which also provided dynamic

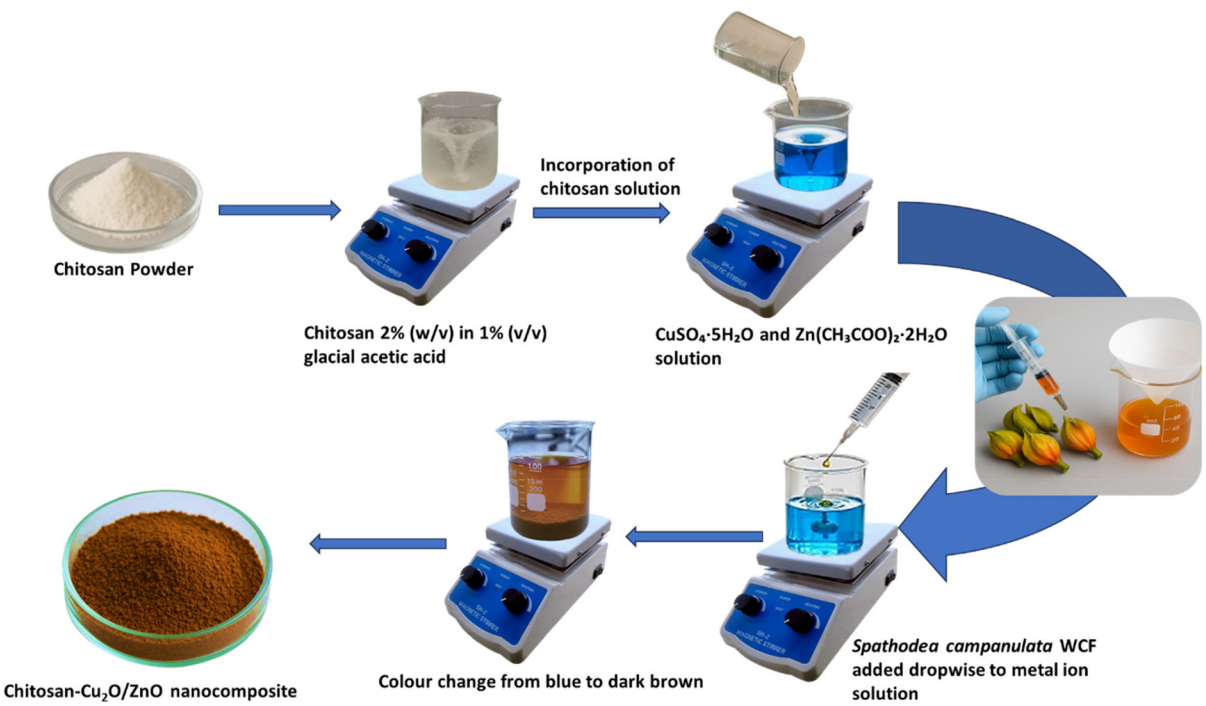

Scheme 1 Schematic illustration of the green synthesis of CS-Cu_2O/ZnO NC.

light scattering (DLS) measurements for determining the hydrodynamic particle size distribution.

2.5. Drug loading and *in vitro* release studies

2.5.1. Cisplatin coated with metal-NPs and loading on chitosan. Loading of cisplatin on chitosan coated metal nanoparticles was carried out according to Goa *et al.* and Mohammadi-Samani *et al.* Metal-nanocomposite (50 mg) was added to 2% glacial acetic acid solution (100 ml) containing high molecular weight chitosan (310–375 KDa, purchased from Sigma Aldrich) and mixed overnight. Cisplatin (4 mg) was added to prepared solution (70 ml) for 48 hours. The free cisplatin was removed by ultracentrifugation at 15 000 rpm for 5 min at 4 °C. After ultracentrifugation, the supernatant liquid was removed then cisplatin/CS-Cu_2O/ZnO NC were suspended in sterilized phosphate buffered saline (PBS).

2.5.2. Assessment of cisplatin loading efficiency and its release from chitosan coated Cu_2O/ZnO NC delivery system. The amount of unloaded cisplatin was measured after releasing from metal NPs by reading the absorbance at 302 nm of the supernatant using UV spectroscopy. The cisplatin loading efficiency (LE) of the chitosan-coated metal nanoparticles was calculated as LE % = (total added cisplatin − unloaded cisplatin)/total added cisplatin. Cisplatin loaded on chitosan coated metal nanoparticles was suspended in phosphate buffered saline medium, pH 7.4 at 37 °C with total volume 50 ml. The mixture was stirred at 120 rpm with magnet stirrer at 37 °C. One ml of cisplatin releasing medium was withdrawn then read at 302 nm and one ml of fresh PBS was replaced. This step was repeated intervals every 12 hours for 72 hours. The Cumulative percentage release and concentration of cisplatin in sample were calculated.

2.6. Anticancer activity and toxicity

In the present study the developed cisplatin loaded CS-Cu_2O/ZnO NC were evaluated for the anticancer activity against fibroblast cell line L929 and skin cancer A375 cell line by using MTT [2-(4,5-dimethylthiazol-2-yl)-3,5-diphenyl-2*H*-tetrazol-3-ium bromide] calorimetric assay. The different concentrations of (20 μg, 40 μg, 60 μg, 80 μg and 100 μg) proposed composite was tested on L929 cell line and for skin cancer A375 cell line (10 μg, 20 μg, 30 μg, 40 μg and 50 μg) were treated. Initially by using DMEM (Dulbecco's Modified Eagle Medium) with 10% FBS the monolayer cell culture was trypsinized and the cell count was adjusted to 1.0×10^5 cells per mL. Further it was transferred to 96-well microliter plates for growth (Falcon, Becton–Dickinson, Franklin Lakes, NJ, USA). After 24 hours of incubation, the used media was taken out and fresh media was added along with proposed test samples. After 24 hours incubation with drugs the media with drugs were removed and subjected for the MTT (200 μL) treatment for 3 hours, after incubation DMSO was added to dissolve the formazan salt that formed was quantified at 595 nm (Bio-Rad Laboratories, Inc., Hercules, CA, USA). The formula below was used to calculate the percentage growth inhibition, and the dose–response curves for each cell line were used to determine the concentration of test medication needed to inhibit cell growth by 50% (IC_{50}). This test is based on the reduction of MTT to a purple formazan product by intact cells mitochondrial dehydrogenase. Percentage inhibition was calculated as follows.

$$\text{Inhibition percentage} = \text{OD of test sample} \div \text{OD of control} \times 100$$

2.7. *In vitro* wound healing scratch assay test

In the present study the known concentration of proposed composite (7.45 μg) was tested for spreading and migration properties of the cells of L929 cell line induced by these samples. Initially the cells were grown into the 12 well animal cell culture plates which contain the DMEM media supplemented with 10% FBS along with 2% of penstrip antibiotic. Once after reaching the complete growth with around 50 000 cells density *i.e.* formation of monolayer confluent of cells by using a sterile 100 μL plastic pipette tip scratch was made. Unwanted cell debris were washed away with help of PBS solution. Further the cells were treated with different testing polymer samples of known concentration and for negative control untreated cells were considered whereas for positive control standard ascorbic acid was taken. The cells were then incubated for 24 h at 37 °C with 5% CO_2. The scratched cell layers incubated at different intervals from 0 h, 12 h and 24 h cells photographed and used for the study of relative cell migration and wound closure. The gap distance was quantitatively evaluated using MagVision Software by measurement calibration at 4× resolution. The wound closure and rate of migration was calculated using following formula:

$$\text{Wound closure } (\%) = A_{0\ \mathrm{h}} - A_{T\ \mathrm{h}}/A_{T\ \mathrm{h}} \times 100$$

$$R_{\mathrm{m}}\ (\text{rate of migration}) = W_{\mathrm{i}} - W_{\mathrm{f}}/T$$

wherein $A_{0\ \mathrm{h}}$ = area of the wound was measured immediately after scratching, $A_{T\ \mathrm{h}}$ = area of the wound measured after the scratch is performed h hours, R_{m} = rate of migration (μm h^{-1}), W_{i} = initial wound width (μm); W_{f} = final wound width (μm) and T = duration of migration (hour).

2.8. Statistical analysis

All the experiments were performed in triplicates and represented as mean with standard error. Further significance of experiment was analysed through one way ANOVA analysis using SPSS.20 version with significant P value (0.01 and 0.05).

3. Results and discussion

3.1. Visual observation and preliminary confirmation

The formation of the CS-Cu_2O/ZnO nanocomposite was preliminarily indicated by a noticeable color change in the reaction mixture from pale blue to reddish-brown, suggesting the reduction of Cu^{2+} and Zn^{2+} ions during the synthesis process. Such color variation is commonly reported in green-mediated nanoparticle synthesis and reflects the interaction between

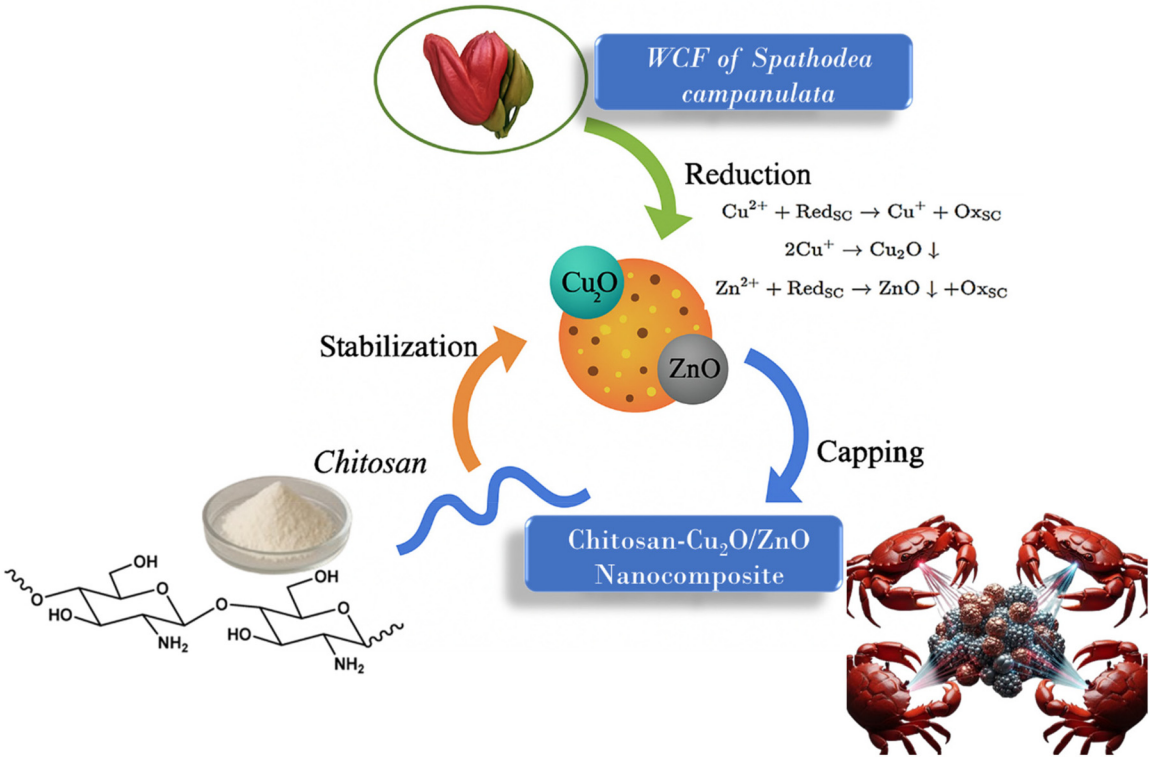

Fig. 1 Proposed mechanism for the green synthesis of chitosan-anchored Cu_2O/ZnO nanocomposite (CS-Cu_2O/ZnO NC) using WCF as a bioreductant and stabilizing agent.

metal ions and bioactive phytochemicals. The phytoconstituents present in the water calyx fluid (WCF) of *Spathodea campanulata* flower buds are known to act as natural reducing and stabilizing agents, facilitating the formation of the nanocomposite. Furthermore, the presence of chitosan contributed to the effective capping and stabilization of the nanoparticles, thereby promoting improved dispersion and colloidal stability of the CS-Cu_2O/ZnO nanocomposite.

3.2. Mechanism of WCF of *Spathodea campanulata* in nanocomposite synthesis

The water calyx fluid (WCF) of *Spathodea campanulata* plays a crucial dual role in the green synthesis of the CS-Cu_2O/ZnO NC functioning as both a reducing agent and a stabilizer. Phytochemical screening studies have shown that the WCF from *S. campanulata* buds is rich in polyphenols, flavonoids, alkaloids, terpenoids, and tannins, all of which contribute functional groups such as hydroxyl (–OH), carboxyl (–COOH), and carbonyl (C═O) moieties (SI, Table S1). These groups actively participate in the reduction of metal precursors and in capping the nascent nanoparticles to prevent agglomeration (Table S2).

3.2.1. Reduction of metal ions. In the synthesis process, aqueous solutions of $CuSO_4 \cdot 5H_2O$ and $Zn(CH_3COO)_2 \cdot 2H_2O$ are mixed with the WCF under ambient conditions. The bioactive molecules in the extract reduce Cu^{2+} to Cu^{+} (leading to Cu_2O formation) and Zn^{2+} to ZnO nanoparticles. The mechanism primarily involves the donation of electrons from phenolic –OH groups or flavonoid structures:

$$Cu^{2+} + Red_{SC} \rightarrow Cu^{+} + Ox_{SC}$$

$$2Cu^{+} \rightarrow Cu_2O \downarrow$$

$$Zn^{2+} + Red_{SC} \rightarrow ZnO \downarrow + Ox_{SC}$$

Here, Red_{SC} refers to the reducing phytoconstituents (*e.g.*, flavonoids or tannins), and Ox_{SC} is their corresponding oxidized form. This redox conversion facilitates the nucleation and controlled growth of metal oxide nanoparticles *in situ* (Fig. 1).

3.2.2. Stabilization and capping. Once reduced, the freshly formed Cu_2O and ZnO nanoparticles are rapidly capped by the same phytoconstituents. Hydroxyl and carbonyl groups from flavonoids or terpenoids form hydrogen bonds or coordinate with the nanoparticle surface, thereby imparting colloidal stability and preventing agglomeration. This stabilizing action is enhanced by chitosan, which simultaneously binds to the nanoparticle surface through its amine ($-NH_2$) and hydroxyl (–OH) functionalities, forming a uniform organic–inorganic hybrid network.

$$Cu_2O/ZnO\text{-NP} + \text{phytochemical}_{SP} \rightleftharpoons \text{capped NP}$$

$$\text{Capped NP} + \text{chitosan-NH}_2 \rightarrow \text{hybrid nanocomposite}$$

The synergy between phytochemicals and chitosan ensures a stable nanosystem with biocompatible surface properties, suitable for biomedical applications such as drug delivery.

3.2.3. Integrated role in composite formation. Overall, the WCF of *Spathodea campanulata* flower bud reduces metal ions to their respective oxides under mild conditions, eliminates the need for toxic chemical reducing agents, and simultaneously stabilizes the nanostructures. Its integration with chitosan enhances nanoparticle dispersion and biocompatibility, producing a robust and multifunctional nanocomposite with potential for targeted therapeutic delivery.

3.3. Structural and morphological characterization

Scanning electron microscopy (SEM) corroborated the TEM observations, revealing aggregated nanoparticulate clusters with a rough, irregular surface morphology, characteristic of polymer-stabilized inorganic nanostructures (Fig. 2A and B). Energy Dispersive X-ray Spectroscopy (EDX), coupled with SEM, was used to confirm the elemental composition of the nanocomposite. The EDX spectrum displayed prominent signals corresponding to copper (Cu), zinc (Zn), and oxygen (O), validating the formation of Cu_2O and ZnO phases (Fig. 2C). Additionally, the presence of carbon (C) and nitrogen (N) peaks confirmed the successful incorporation of chitosan, while trace elements from the plant extract may also have contributed to minor signals. The elemental mapping further demonstrated uniform distribution of Cu and Zn across the composite matrix, suggesting homogeneous integration of both metal oxides. Transmission electron microscopy (TEM) images revealed uniformly dispersed, quasi-spherical nanoparticles embedded within a polymeric matrix, with particle sizes ranging from 20 to 40 nm with an average particle size of 30 ± 5 nm (Fig. 2D). The particles exhibited minimal aggregation, suggesting effective capping and stabilization by chitosan and phytochemicals from WCF. A clear core–shell-like contrast was observed in some regions, potentially indicating the formation of a chitosan coating around the Cu_2O/ZnO nanostructures. This matches the histogram, where the highest frequency is centered around the 30–40 nm range, confirming a moderate size distribution (Fig. 2E). Thus, the histogram quantitatively supports the TEM results, indicating that the synthesized nanoparticles are fairly uniform with slight polydispersity.

The structural integrity and morphological attributes of the synthesized CS-Cu_2O/ZnO NC were systematically examined using a suite of advanced analytical techniques. X-ray diffraction (XRD) analysis revealed well-defined diffraction peaks corresponding to the crystalline phases of both Cu_2O and ZnO (Fig. 3A). The peaks observed at 2θ values around 29.5°, 36.4°, 42.3°, and 61.4° were indexed to the (110), (111), (200), and (220) planes of cubic Cu_2O (JCPDS No. 05-0667), while the reflections at 31.7°, 34.3°, and 36.2° were assigned to the (100), (002), and (101) planes of hexagonal ZnO (JCPDS No. 36-1451). The absence of extraneous peaks indicated high phase purity and the successful co-existence of Cu_2O and ZnO within a single composite system. The broadening of peaks further implied the nanocrystalline nature of the material. UV-Visible spectroscopic analysis demonstrated a broad absorption band

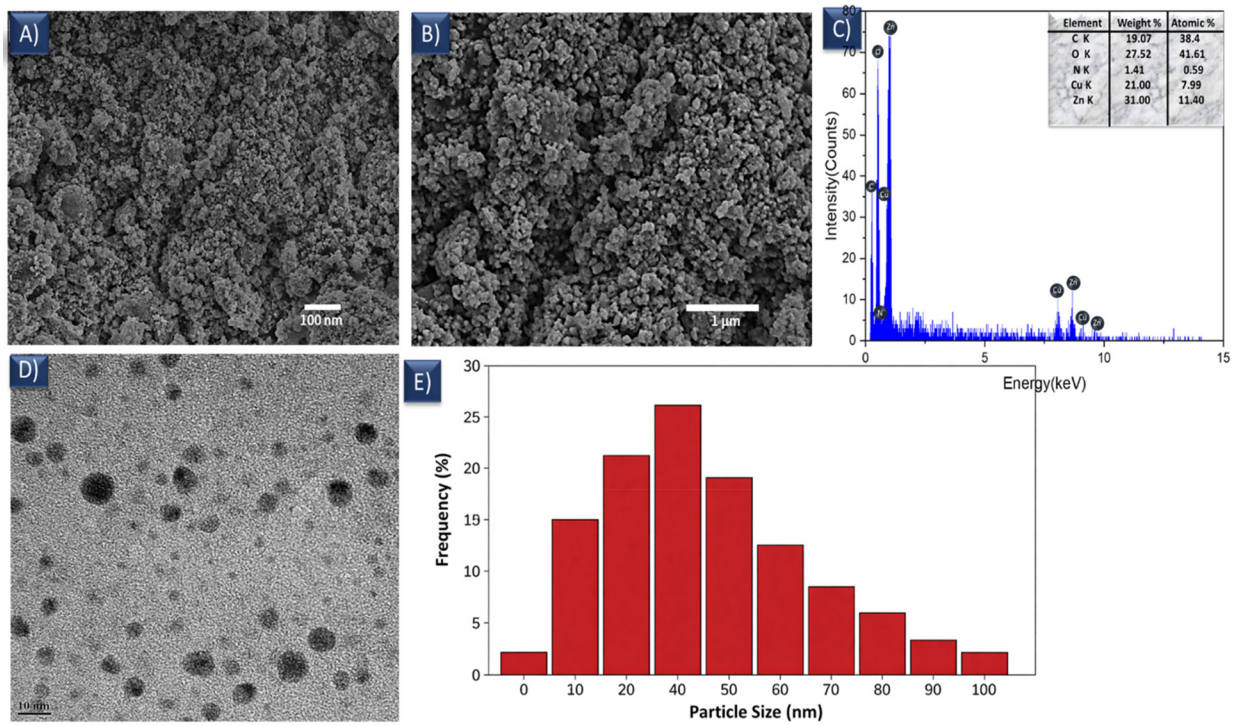

Fig. 2 (A) and (B) FESEM images (C) EDX pattern (D) TEM image (E) histogram of the synthesized CS-Cu_2O/ZnO NC.

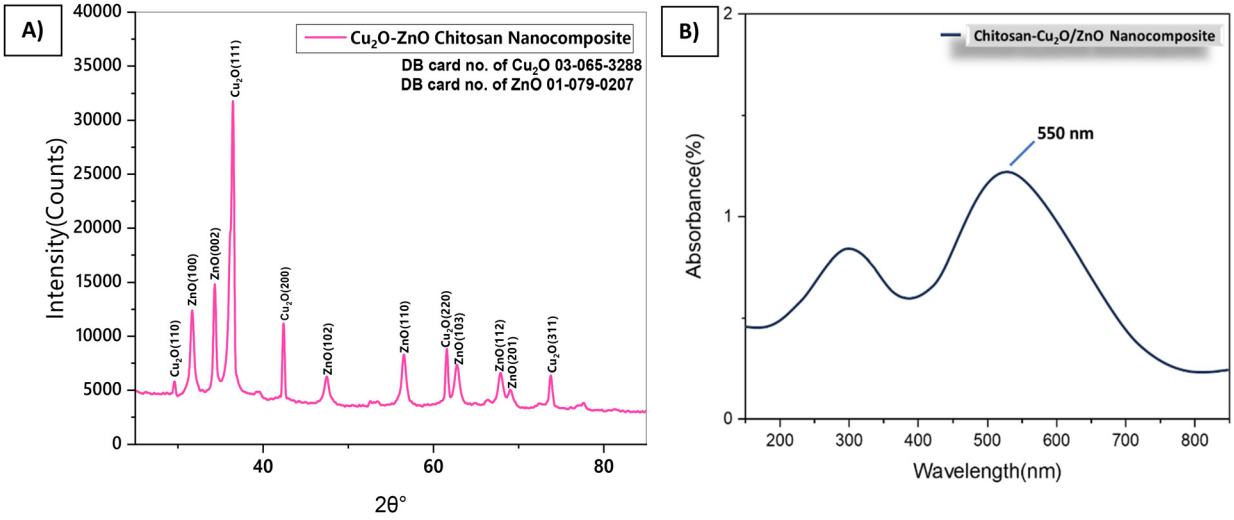

Fig. 3 (A) XRD and (B) UV-visible spectrum of CS-Cu_2O/ZnO NC.

in the range of 270–320 nm, attributed to the interband transitions of ZnO and Cu_2O nanoparticles (Fig. 3B). A bathochromic shift compared to individual precursors at 550 nm suggested potential electronic interactions or coupling effects between the two metal oxides, as well as surface modification by chitosan and plant-derived phytoconstituents. These observations were consistent with successful composite formation. Additionally, the UV-Visible spectrum of WCF was recorded, revealing peaks between 270–290 nm, which correlate with the phytochemical constituents involved in the reduction and stabilization process (Fig. S4).

Fourier-transform infrared (FTIR) spectroscopy provided insight of chitosan (Fig. 4a) and into the chemical interactions within the composite (Fig. 4b). Characteristic bands observed at 3296 cm^{-1} and 1630 cm^{-1} were attributed to O–H/N–H stretching and amide I vibrations, respectively, indicative of chitosan functional groups. A band near 1380 cm^{-1} corresponded to C–N stretching, while strong absorption bands in the fingerprint region around 540–600 cm^{-1} were assigned to metal–oxygen (Cu–O and Zn–O) stretching vibrations. The presence of these bands confirmed effective incorporation of both metal oxides and successful stabilization *via* chitosan and biomolecules from the WCF (Fig. S5).

Atomic force microscopy (AFM) analysis further provided detailed insights into the surface topography, revealing nanoscale granularity and surface elevations. The chitosan coating contributed to the topographical smoothness and increased surface area, which are beneficial for drug adsorption and release kinetics (Fig. 5A). Dynamic light scattering (DLS) measurements indicated a hydrodynamic diameter of approximately 89.3 nm, which was larger than the core sizes observed in TEM. This discrepancy is attributed to the hydrated chitosan layer surrounding the nanocomposite in suspension (Fig. 5B). Zeta potential analysis yielded a negative surface charge of −29.4 mV, signifying steady colloidal stability. The negative charge is likely derived from the deprotonated functional groups of chitosan and phytochemicals, providing electrostatic repulsion that prevents particle aggregation (Fig. 5C). Collectively, these findings confirm the successful green synthesis of a stable, nanoscale, CS-Cu_2O/ZnO NC with well-defined crystalline structure, favourable morphology, and surface characteristics conducive to drug loading and biomedical applications.

3.4. Drug delivery

Cisplatin is a widely used chemotherapeutic agent that has been approved for the treatment of various types of cancer, including bladder, ovarian, testicular, cervical, head and neck, and non-small cell lung cancer.[63] However, the clinical use of cisplatin is limited by its severe systemic toxicity, such as neurotoxicity, ototoxicity, gastrointestinal disturbances, myelosuppression, and nephrotoxicity.[64] To overcome these limitations, researchers have explored the use of nanoparticle-based drug delivery systems as a strategy to improve the therapeutic efficacy and reduce the toxicity of cisplatin. In this study, we investigated the use of CS-Cu_2O/ZnO NC as a drug delivery system for cisplatin. Chitosan is a natural polysaccharide with excellent biocompatibility, biodegradability, and mucoadhesive properties, making it an attractive material for drug delivery applications. The incorporation of Cu_2O and ZnO nanoparticles into the chitosan matrix can potentially enhance the drug delivery capabilities of the system, as these nanoparticles have been shown to possess various biological activities, including antimicrobial, anti-inflammatory, and anticancer properties. The strategic application of the synthesized CS-Cu_2O/ZnO NC as a drug delivery carrier was demonstrated through cisplatin loading and *in vitro* release studies. Cisplatin, a potent chemotherapeutic agent, was selected as the model drug owing to its widespread clinical use and known limitations, including poor selectivity and systemic toxicity. The nanocomposite matrix offered a multifunctional platform for cisplatin immobilization, leveraging chitosan's

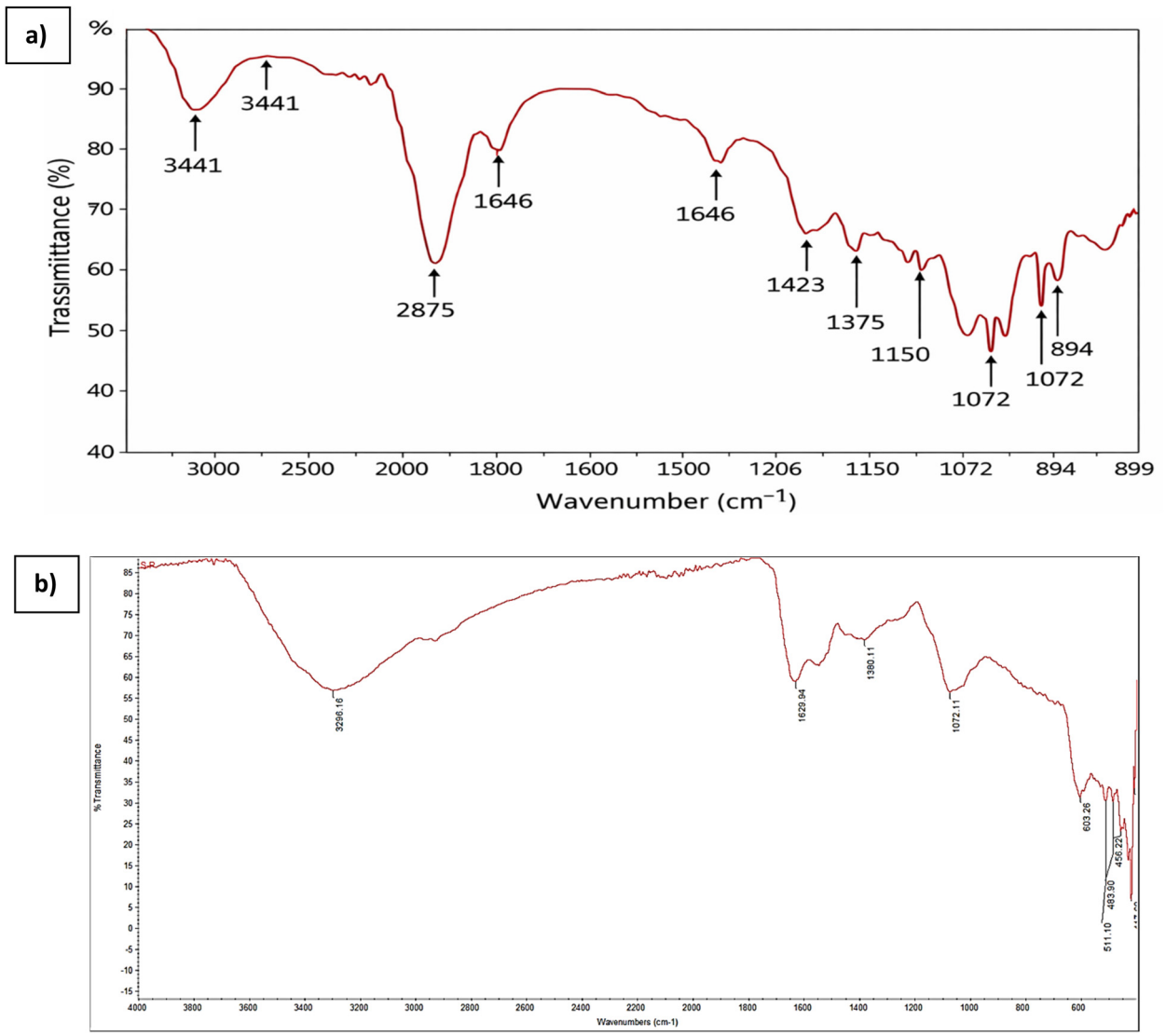

Fig. 4 FTIR of (a) chitosan (b) CS-Cu_2O/ZnO NC.

mucoadhesive and ion-binding properties alongside the structural support and bioactivity of metal oxides.

Drug loading efficiency was found to be high, attributable to the electrostatic interactions between the protonated amino groups of chitosan and the negatively charged cisplatin molecules, as well as possible coordination with Cu and Zn oxide domains. The uniformly distributed surface features observed in AFM and TEM imaging further suggest increased surface area for drug entrapment, while the porosity introduced by the chitosan network likely facilitated deep diffusion and retention of the drug within the composite structure. The *in vitro* release profile of cisplatin from the nanocomposite revealed a biphasic pattern typical of smart polymer-based delivery systems.

Moreover, the hybrid nature of the composite wherein the metal oxides not only enhance structural robustness but also interact with the drug *via* coordination or hydrogen bonding contributes to a controlled delay in drug release. Such tunable release characteristics are highly desirable for chemotherapeutics, where maintaining effective drug concentrations at the tumor site while minimizing off-target effects is critical. Notably, the nanoscale size (89.3 nm hydrodynamic diameter) and surface charge (−29.4 mV) of the drug-loaded composite ensure enhanced colloidal stability and prolonged circulation, increasing the likelihood of tumor accumulation *via* the enhanced permeability and retention (EPR) effect. The successful demonstration of controlled, sustained cisplatin release highlights the potential of this green-engineered nanocomposite as a next-generation smart drug delivery system capable of improving therapeutic outcomes in cancer treatment.

3.4.1. Mechanism of action: cisplatin release from chitosan-Cu_2O/ZnO nanocomposite (drug loading efficiency)

3.4.1.1. Drug loading via electrostatic and coordination interactions. The initial step in the drug delivery process involves

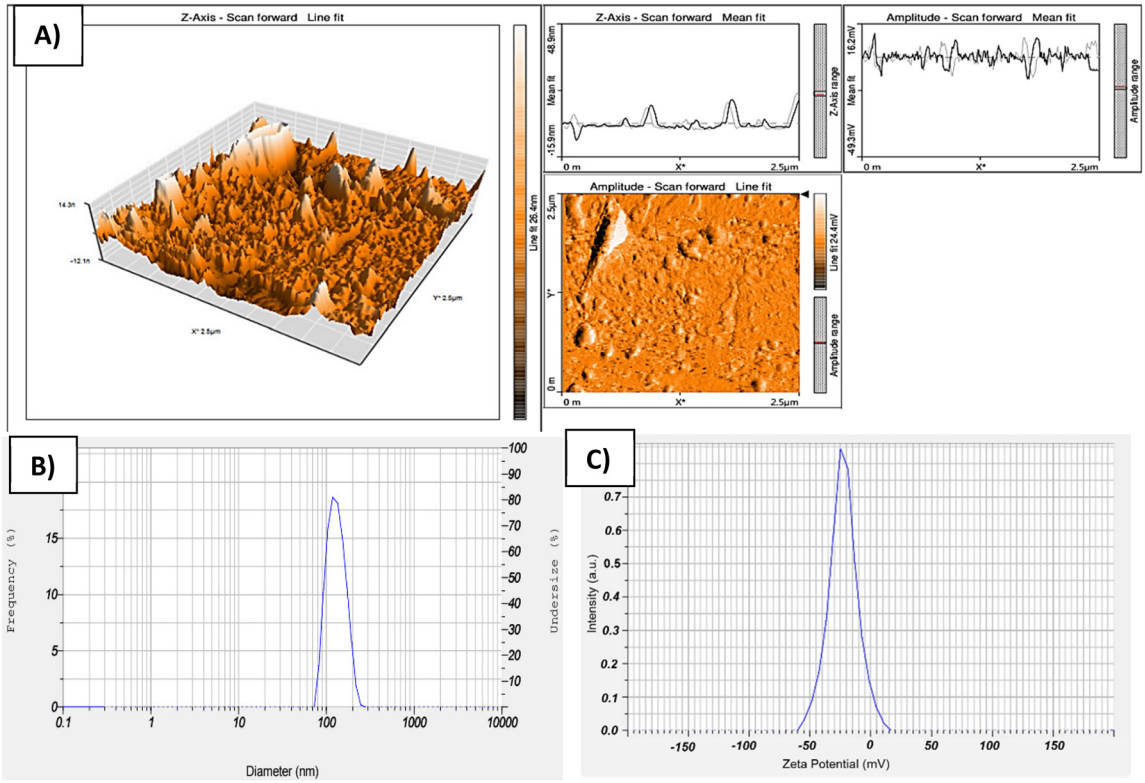

Fig. 5 (A) AFM, (B) particle size and (C) zeta potential of CS-Cu_2O/ZnO NC.

the efficient encapsulation of cisplatin (*cis*-$[PtCl_2(NH_3)_2]$) within the CS-Cu_2O/ZnO NC. Chitosan, a cationic polysaccharide, contains abundant amino ($-NH_2$) and hydroxyl (–OH) functional groups that serve as interactive sites for drug molecules. In slightly acidic conditions (acetic acid medium), the amino groups become protonated to form $-NH_3^+$, enabling electrostatic attraction with the negatively charged regions of cisplatin. This non-covalent interaction enhances the binding affinity of cisplatin to the polymer matrix:

$$\text{Chitosan} - NH_3^+ + cis - [PtCl_2(NH_3)_2] \rightleftharpoons \text{chitosan} - NH_3^+ \cdots PtCl_2(NH_3)_2$$

In addition, the oxygen-rich surfaces of Cu_2O and ZnO nanoparticles present in the composite offer coordination sites capable of forming weak bonds with the platinum center of cisplatin, further stabilizing the loaded drug. This is supported by the formation of surface-bound complexes:

$$\text{Metal} - \text{OH (Cu or Zn)} + cis\text{-}[PtCl_2(NH_3)_2] \rightarrow \text{metal} - O - PtCl(NH_3)_2 + HCl$$

These interactions ensure high drug loading efficiency while preserving the bioactivity of both cisplatin and the carrier matrix.

3.4.1.2. pH-Responsive swelling and triggered drug release. The release of cisplatin from the nanocomposite is primarily governed by the pH sensitivity of chitosan and the microenvironmental conditions at the target site. Under physiological pH (7.4) or mildly acidic tumor pH (5.5–6.8), the amino groups of chitosan undergo further protonation, leading to increased electrostatic repulsion within the polymer chains. This results in polymer chain relaxation, water uptake, and swelling of the chitosan matrix, which collectively facilitate the outward diffusion of cisplatin molecules:

$$\text{Chitosan} - NH_3^+ \cdots PtCl_2(NH_3)_2 + H_2O \rightarrow \text{chitosan} - NH_3^+ + PtCl_2(NH_3)_2$$

This mechanism leads to an initial burst release often attributed to surface-bound drug followed by a sustained release phase as the drug diffuses through the hydrated polymeric network (Fig. 6). The rate of release can be finely tuned by adjusting chitosan concentration, nanoparticle dispersion, and the environmental pH. Importantly, this pH-triggered mechanism ensures selective release at the acidic tumor site while minimizing premature drug leakage in healthy tissues.

3.4.1.3. Synergistic contribution of Cu_2O/ZnO nanoparticles. Beyond their structural role in the nanocomposite, the embedded Cu_2O and ZnO nanoparticles may actively contribute to the therapeutic efficacy through reactive oxygen species (ROS) generation under biological conditions. Cu^+ and Zn^{2+} ions can participate in redox reactions within the cellular environment, particularly in the presence of intracellular glutathione or peroxides, producing hydroxyl radicals ($^{\bullet}OH$) and superoxide anions ($O_2^{\bullet-}$). These ROS can damage cancer cell

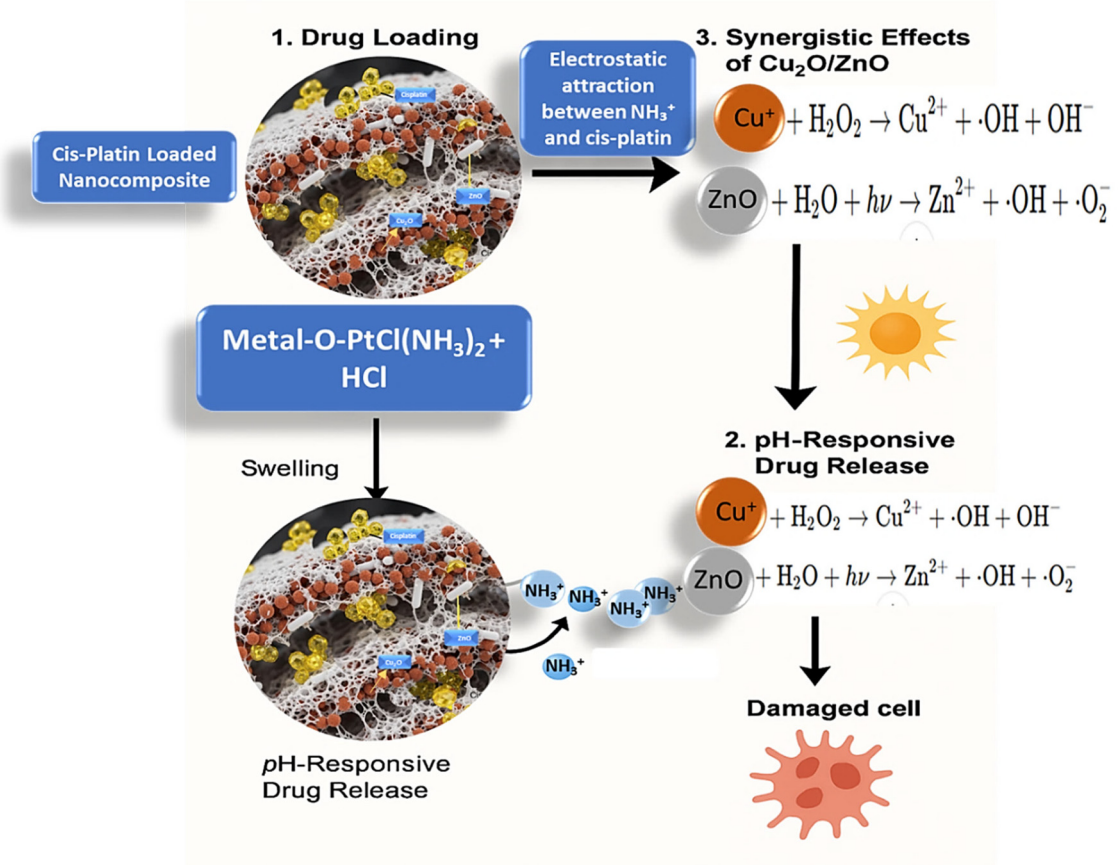

Fig. 6 Mechanism of drug loading and release.

membranes, proteins, and DNA, enhancing the cytotoxic effect of cisplatin:

$$Cu^{+} + H_2O_2 \rightarrow Cu^{2+} + {}^{\bullet}OH + OH^{-}$$

$$ZnO + H_2O + h\nu \rightarrow Zn^{2+} + {}^{\bullet}OH + {}^{\bullet}O_2{}^{-}$$

This dual mode of action cisplatin-mediated DNA damage and ROS-induced oxidative stress can work synergistically to induce apoptosis in cancer cells. Moreover, the metal oxide phase provides mechanical stability to the nanocomposite and acts as a gatekeeper to modulate drug release *via* redox-sensitive degradation pathways. Thus, the CS-Cu_2O/ZnO NC operates as a multifunctional theranostic platform combining targeted drug delivery, sustained release, and intrinsic bioactivity.

3.4.2. *In vitro* drug release studies. In the present study the drug release assay showed that with the increase in the duration the percentage of drug release was increased. An initial burst release of 39.35 ± 0.12% was observed within the first 12 hours, which may be attributed to the desorption of surface-adsorbed cisplatin. This was followed by a sustained release phase, culminating in 94.88 ± 0.22% cumulative release over 72 hours under physiological conditions (PBS, pH 7.4). The results are shown in Table 2 and Fig. 7. The release behavior can be ascribed to a combination of Fickian diffusion and polymer relaxation-driven mechanisms. Chitosan's pH-responsiveness played a pivotal role, as mild swelling in the physiological buffer facilitated gradual expansion of the matrix and progressive drug liberation. These findings are consistent with previous studies that have reported the successful encapsulation of cisplatin in nanoparticle-based drug delivery systems. The polymer-based nanoparticles, such as polymeric micelles and hydrogels, have been shown to improve the pharmacokinetics and biodistribution of cisplatin, leading to enhanced antitumor activity and reduced systemic toxicity.

Table 2 Amount of Drug release from the proposed nano drug system (the results are expressed as triplicates mean ± standard deviation)

Sl. no	Duration in hours	Percentage of drug release
1	12	39.35 ± 0.1230
2	24	62.86 ± 0.1508
3	36	75.88 ± 0.2144
4	48	88.19 ± 0.1639
5	60	91.44 ± 0.1520
6	72	94.88 ± 0.2288

Copper oxide (Cu_2O) and zinc oxide (ZnO) nanoparticles have emerged as highly promising candidates in the biomedical field due to their distinctive physicochemical properties, low cost, and broad spectrum of biological activities. These metal oxide nanoparticles exhibit remarkable anti-

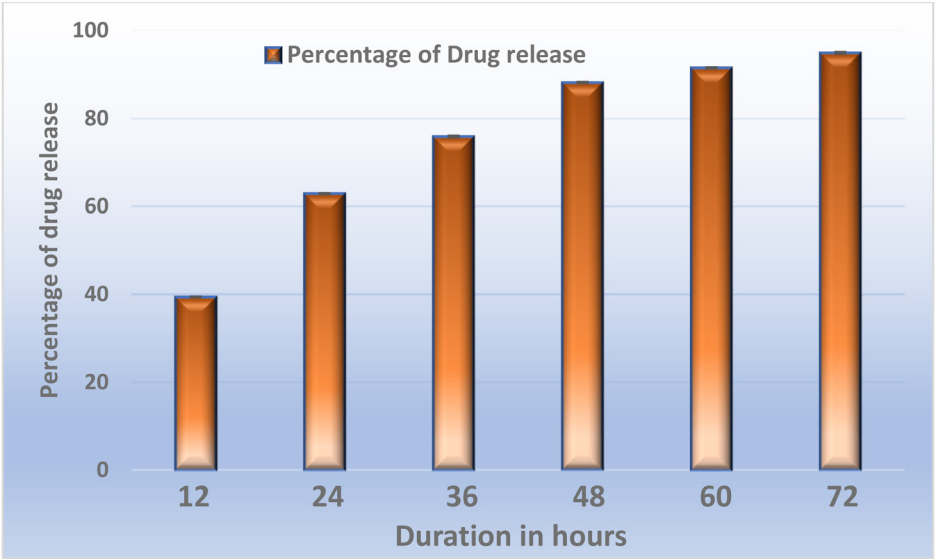

Fig. 7 Amount of drug release from the proposed nano drug system.

microbial, antioxidant, anticancer, and imaging capabilities, making them suitable for a wide range of medical applications.[65,66] Among metal oxides, Cu_2O and ZnO stand out for their ease of synthesis, stability, and strong interaction with biological systems, often outperforming more expensive counterparts like silver and gold nanoparticles. Chitosan, a natural polysaccharide obtained through the deacetylation of chitin found in crustacean exoskeletons, has garnered attention for its intrinsic biocompatibility, biodegradability, mucoadhesive nature, and antimicrobial activity. When combined with metal oxide nanoparticles such as Cu_2O and ZnO, chitosan not only enhances the dispersion and stability of the nanomaterials but also imparts additional functional properties, creating a synergistic effect ideal for biomedical applications. Chitosan-conjugated Cu_2O/ZnO nanocomposites have shown potent antimicrobial activity against a diverse array of pathogenic bacteria, fungi, and viruses, primarily through mechanisms involving the generation of reactive oxygen species (ROS), disruption of microbial membranes, and interference with microbial DNA.[65] These properties render the nanocomposites highly suitable for applications in wound healing, antimicrobial coatings for medical devices, and water purification systems.

Beyond antimicrobial efficacy, Cu_2O/ZnO-chitosan nanocomposites have also demonstrated notable anticancer potential. Several studies have reported their selective cytotoxicity against cancer cells while minimizing damage to normal cells, attributed to the induction of oxidative stress, mitochondrial dysfunction, and apoptosis pathways.[67] Furthermore, these nanomaterials have shown anti-angiogenic properties, which are essential for inhibiting tumor growth and metastasis.[68] This study aimed to assess the toxic impact of Cu_2O and ZnO nanoparticles conjugated with chitosan on the L929 fibroblast cell line using the MTT assay. The results revealed that as the concentration was increased *i.e.*, more than 80 μg the toxic nature was seen with the percentage of cell viability 49.72 ± 1.6501 and for higher concentration *i.e.*, 100 μg it was decreased to 27.17 ± 1.7601. Whereas for initial lower concentrations *viz.*, 20 μg, 40 μg and 60 μg the percentage of cell viability was found to be 89.32 ± 0.9901, 74.91 ± 1.7601 and 63.03 ± 0.6600 respectively. The standard drug cisplatin has shown around 8.69 ± 0.8800. The IC_{50} was found to be 74.50 μg ml^{-1}. These findings concluded that the proposed nano composite system exhibited toxicity at only higher dosage of concentrations whereas for lower concentration it was found to be less toxic. The results were shown in Table 3 and Fig. 8. Further, the microscopic based morphological studies correlate with the MTT results *i.e.* in case of at lower concentrations the cells were still intact, healthy with proper morphology whereas at higher concentrations there was change in the cells morphology with the formation of dead cells, cell elongation and reduction in the number of cells. The results were shown in Fig. 9.

3.4.3. Cell viability evaluation. These results indicate that Cu_2O/ZnO nanoparticles exhibit varying degrees of toxicity,

Table 3 Toxicity of CS-Cu_2O/ZnO NC drug delivery system against fibroblast L929 cell line (the results are expressed as triplicates mean ± standard error)

Cell line	Drug	Concentration in μg	Percentage of cell viability	IC_{50} in μg
L929	CS-Cu_2O/ZnO NC	20	89.32 ± 0.9901	74.50
		40	74.91 ± 1.7601	
		60	63.03 ± 0.6600	
		80	49.72 ± 1.6501	
		100	27.17 ± 1.7601	
L929	Cisplatin	15	8.69 ± 0.8800	Less than 20

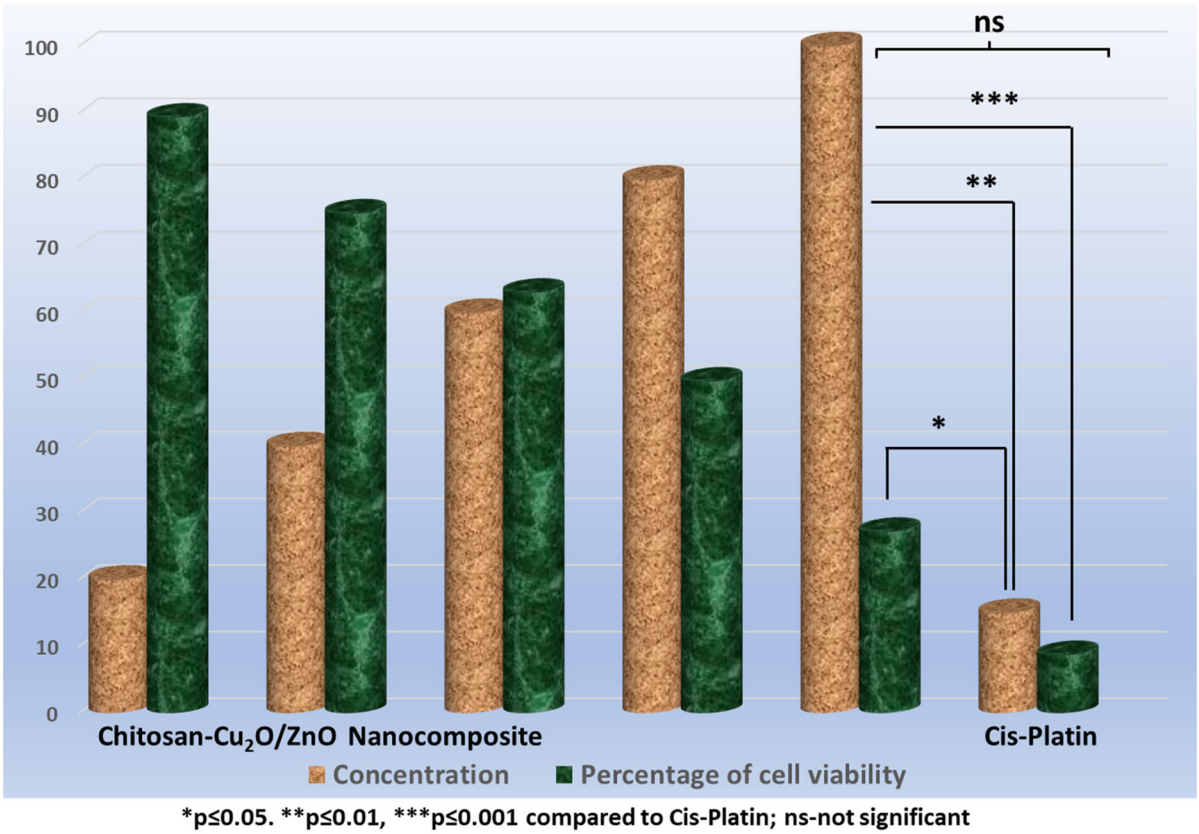

Fig. 8 Toxicity of CS-Cu_2O/ZnO NC drug delivery system against L929 cell line (asterisks (*) indicate statistically significant differences ($p \leq 0.05$) in cell viability between nanocomposite treatments and cisplatin, while "ns" denotes no significant difference, showing comparable results at the highest concentration within a 95% confidence interval).

depending on their physicochemical characteristics and the experimental conditions. Some studies have reported that Cu_2O/ZnO nanoparticles are hypotoxic, while others have shown significant antibacterial effects also, suggesting their potential application in wound-healing preparations.[68]The toxicity of Cu_2O/ZnO nanoparticles is also influenced by factors such as water hardness, alkalinity, presence of organic and inorganic ligands, pH, and temperature.[69] In the context of the L929 fibroblast cell line, the MTT assay was employed to evaluate the cytotoxic effects of Cu_2O/ZnO nanoparticles conjugated with chitosan. The findings from this study will contribute to a better understanding of the biocompatibility and potential applications of copper nanoparticle-based materials in biomedical and tissue engineering applications (Table 4 and Fig. 8).

3.5. Anticancer activity

Skin cancer is a significant public health concern, with the incidence of melanoma, the deadliest form of skin cancer, increasing in recent years[69] Developing effective and safe treatment options is crucial. Copper oxide and zinc oxide nanoparticles have demonstrated promising anticancer properties in previous studies, indicating their potential as a therapeutic agent.[70] In this research, we investigated the anticancer activity of Cu_2O and ZnO nanoparticles conjugated with chitosan against the skin cancer cell line A375. Chitosan was selected as a carrier due to its biocompatibility, biodegradability, and ability to enhance the cellular uptake of nanoparticles.

In the present study the proposed nano conjugated system was evaluated for the anticancer studies against skin cancer A375 cell line along with cisplatin and untreated cells as positive and negative control group. The results revealed that the anticancer activity was found to be dose dependent manner *i.e.*, with the increase in the concentrations of CS-Cu_2O/ZnO NC from 10 μg to 50 μg the percentage of cell viability was found to be decreased. For 10 μg the percentage of cell viability was seen to be 84.48 ± 1.8915 and further at higher concentration 50 μg it was decreased to 15.63 ± 1.1349. For standard drug cisplatin it was found to be 11.72 ± 1.0088. The IC_{50} for CS-Cu_2O/ZnO NC was seen to be 29.84 μg ml^{-1}. The results are shown in Table 3 and Fig. 10. Further, the morphological studies on the A375 cell line at different concentrations have shown the variation in their morphology on comparison with the untreated group of cells. In case of untreated the cells were found to be healthy nucleated and having proper morphology whereas for standard and CS-Cu_2O/ZnO NC there was formation of apoptotic cells, cell shrinkage, cell elongation, cells turgidity. The results were shown in Fig. 11.

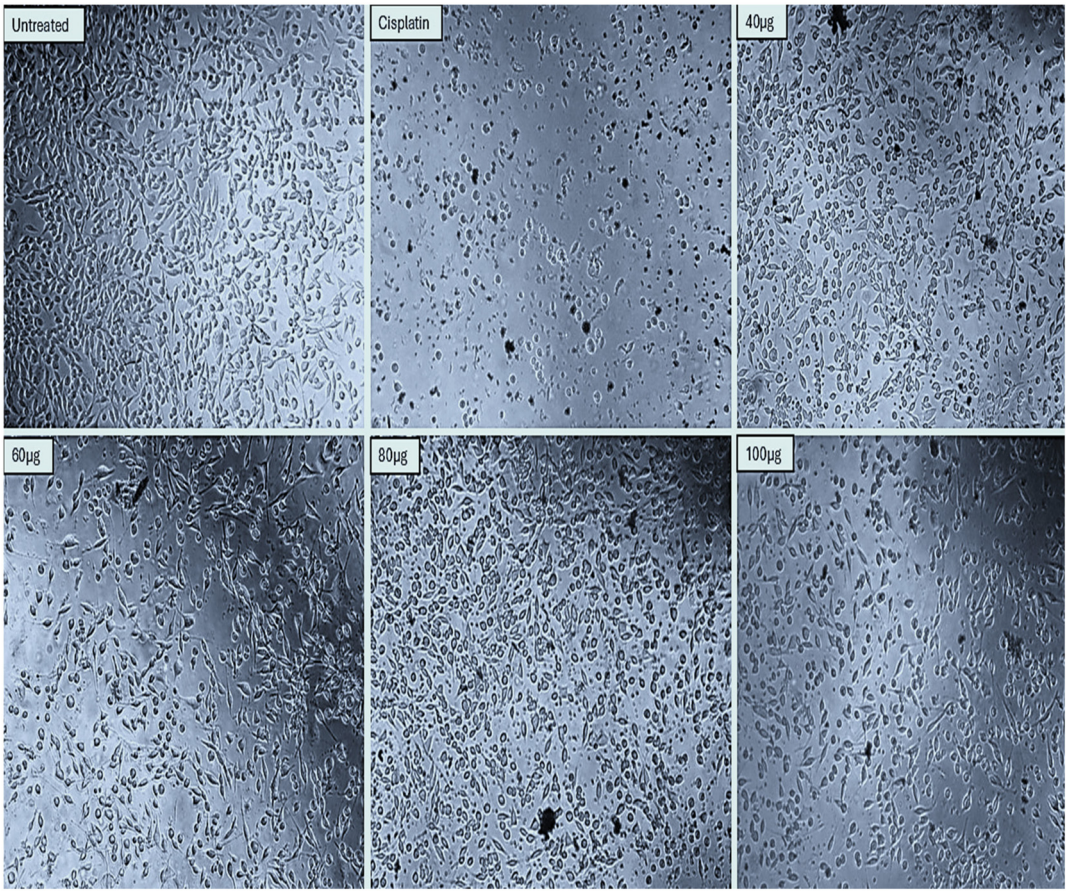

Fig. 9 Morphological effects of CS-Cu_2O/ZnO NC on L929 cell line.

Table 4 Anticancer activity of CS-Cu_2O/ZnO NC drug delivery system against skin cancer A375 cell line

Cell line	Drug	Concentration in µg	Percentage of cell viability	IC_{50} in µg ml^{-1}
A375	Nano composite	10	84.48 ± 1.8915	29.84
		20	65.19 ± 2.0176	
		30	52.20 ± 1.1349	
		40	31.14 ± 0.7566	
		50	15.63 ± 1.1349	
A375	Cisplatin	15	11.72 ± 1.0088	Less than 15

The results are expressed as triplicates mean ± standard error.

3.6. Wound healing activity

One of the foremost biomedical applications of Cu_2O and ZnO nanoparticles lies in their therapeutic efficacy against skin malignancies, particularly the A375 melanoma cell line. Both Cu_2O and ZnO nanoparticles exhibit pronounced cytotoxicity toward A375 cells by inducing apoptosis and suppressing tumor proliferation. The integration of chitosan into their nanostructure further augments biocompatibility, enhances cellular internalization, and facilitates site-specific delivery, thereby amplifying the overall antineoplastic potency. Beyond oncological relevance, the CS-Cu_2O/ZnO nanocomposite also demonstrates substantial potential in wound healing applications. The intrinsic antibacterial activity of Cu_2O and ZnO effectively mitigates the risk of microbial infection, while the regenerative properties of chitosan promote cellular proliferation, tissue remodeling, and accelerated wound closure. This dual functionality underscores the versatility of the nanocomposite as a multifunctional therapeutic platform bridging cancer therapy and regenerative medicine.

3.6.1. Role of ROS in nanocomposite wound healing activity. The wound healing potential of the synthesized Cu_2O/ZnO nanocomposite can be closely associated with the controlled generation of reactive oxygen species (ROS), which play a dual and concentration-dependent role in tissue repair processes. Metal oxide nanomaterials, particularly Cu_2O and ZnO, are known to facilitate the formation of ROS such as superoxide radicals ($O_2^{\bullet -}$), hydroxyl radicals ($^{\bullet}OH$), and hydrogen peroxide (H_2O_2) through redox reactions at their surface. At controlled levels, ROS act as important signaling molecules in wound healing by promoting key physiological events, including cell proliferation, migration, and angiogenesis. These processes are essential for tissue regeneration and remodeling. Additionally, ROS contribute to the activation of growth factors

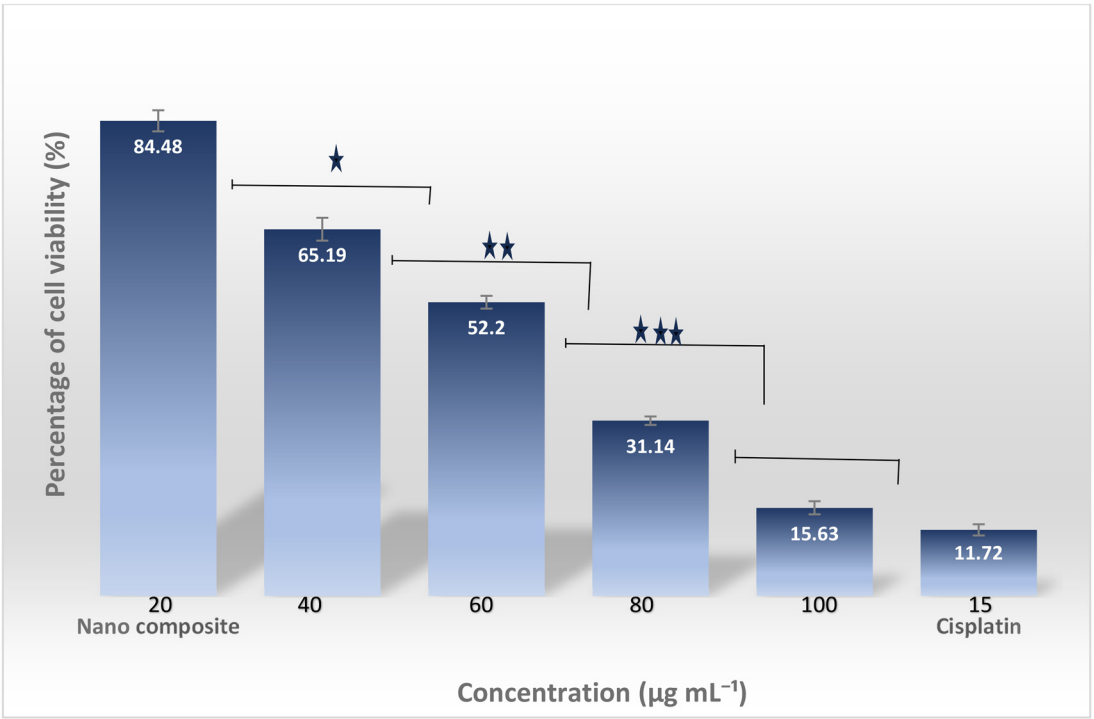

Fig. 10 Anticancer activity of CS-Cu_2O/ZnO NC drug delivery system against skin cancer A375 cell line (data are presented as mean ± SD (n = 3). p < 0.05 indicates a statistically significant difference compared to the 10 μg concentration).

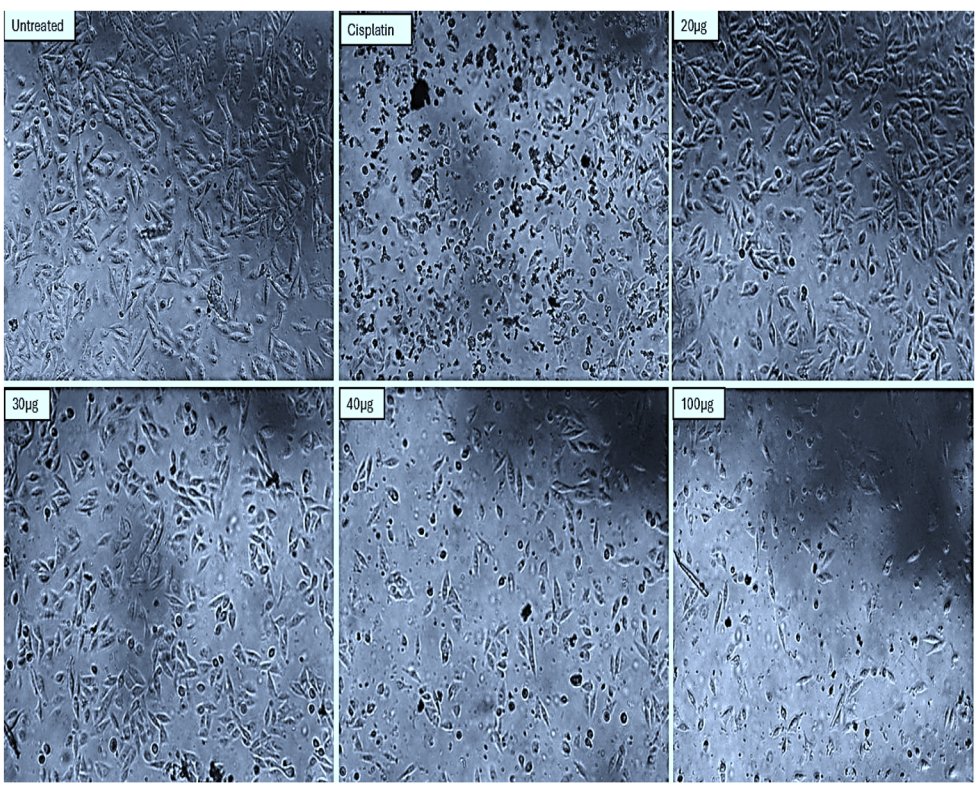

Fig. 11 Morphological effects on cisplatin loaded CS-Cu_2O/ZnO NC on skin cancer A375 cell line.

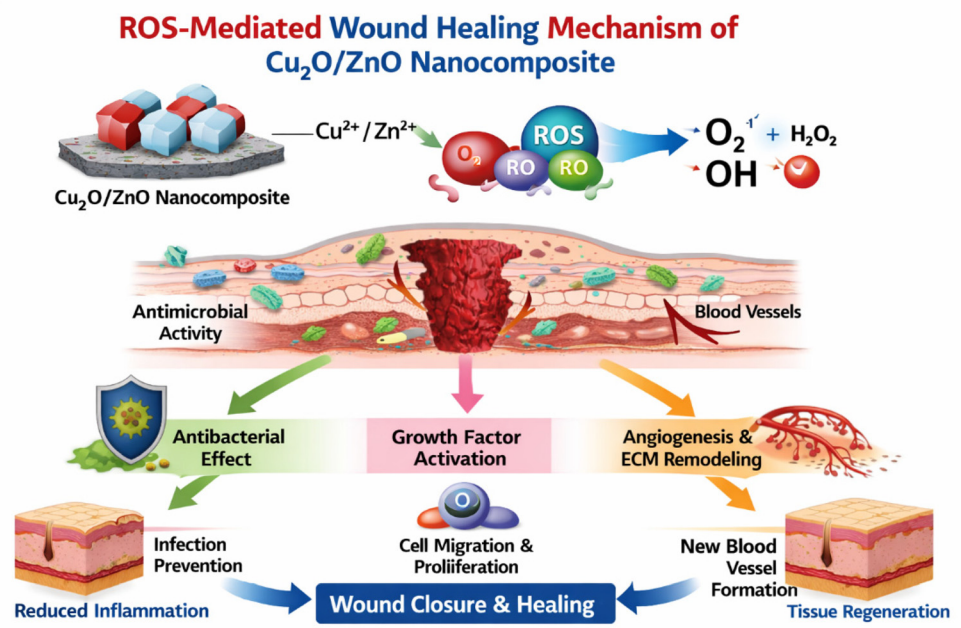

Fig. 12 Schematic illustration of the reactive oxygen species (ROS)-mediated wound healing mechanism of the Cu_2O/ZnO nanocomposite.

and cytokines, which further accelerate the healing cascade.[71–75]

The Cu_2O/ZnO nanocomposite also exhibits antimicrobial activity through ROS-mediated oxidative stress, which helps in preventing infection at the wound site an essential factor for effective healing (Fig. 12). The presence of copper ions further supports angiogenesis and enhances extracellular matrix formation, while ZnO contributes to epithelialization and cell proliferation. Although ROS generation was not directly quantified in the present study, the observed biological responses and established literature strongly support a ROS-mediated mechanism contributing to the wound healing efficacy of the nanocomposite. Future investigations involving quantitative ROS analysis will provide deeper insight into optimizing its therapeutic performance.

3.6.2. *In vitro* scratch assay test. To evaluate the wound-healing efficacy, *in vitro* scratch assays were conducted using the L929 fibroblast cell line. The results demonstrated that the CS-Cu_2O/ZnO nanocomposite (NC) markedly enhanced cellular migration and proliferation, thereby accelerating the closure of the simulated wound.[76–79] In this study, ascorbic acid served as the reference standard and positive control while untreated cells served as negative control, and the nanocomposite was tested at a concentration of 5 μg mL^{-1}. The untreated control group exhibited only 19.78% and 38.87% wound closure at 12 h and 24 h, respectively. By contrast, the standard drug showed 74.40% and 87.52% wound closure over the same time intervals. Remarkably, the CS-Cu_2O/ZnO NC achieved 68.11% closure at 12 h and 82.45% at 24 h, closely approximating the performance of the standard. These findings are summarized in Table 5 and illustrated in Fig. 13. Collectively, the integration of copper oxide and zinc oxide nanoparticles with chitosan has proven effective not only in exerting cytotoxic effects against skin cancer cells but also in promoting wound repair. The synergistic interplay between the bioactive metal oxides and the biopolymer matrix confers enhanced biocompatibility, targeted drug delivery, antimicrobial activity, and regenerative potential. Such multifunctional attributes underscore the promise of CS-Cu_2O/ZnO NCs as a versatile platform for diverse biomedical applications spanning oncological therapy and tissue engineering.

Table 5 Cell migration and wound healing study of CS-Cu_2O/ZnO NC

Treatments	Treating dose in μg	Cell migration in μm after 12 h	Cell migration in μm after 24 h	Percentage of wound closure in after 12 h	Percentage of wound closure after 24 h
CS-Cu_2O/ZnO NC	5	22.04 ± 0.85	14.22 ± 0.62	68.11 ± 2.14	82.45 ± 2.36
Standard (ascorbic acid)	5	24.60 ± 0.91	14.47 ± 0.58	74.40 ± 2.28	87.52 ± 2.41
Untreated	0	9.74 ± 0.48	9.57 ± 0.44	19.78 ± 1.35	38.87 ± 1.72

Values are expressed as mean ± standard deviation (SD) of three independent biological experiments (n = 3), each performed in triplicate. Statistical significance was evaluated using appropriate analysis methods, and differences were considered significant at $p < 0.05$.

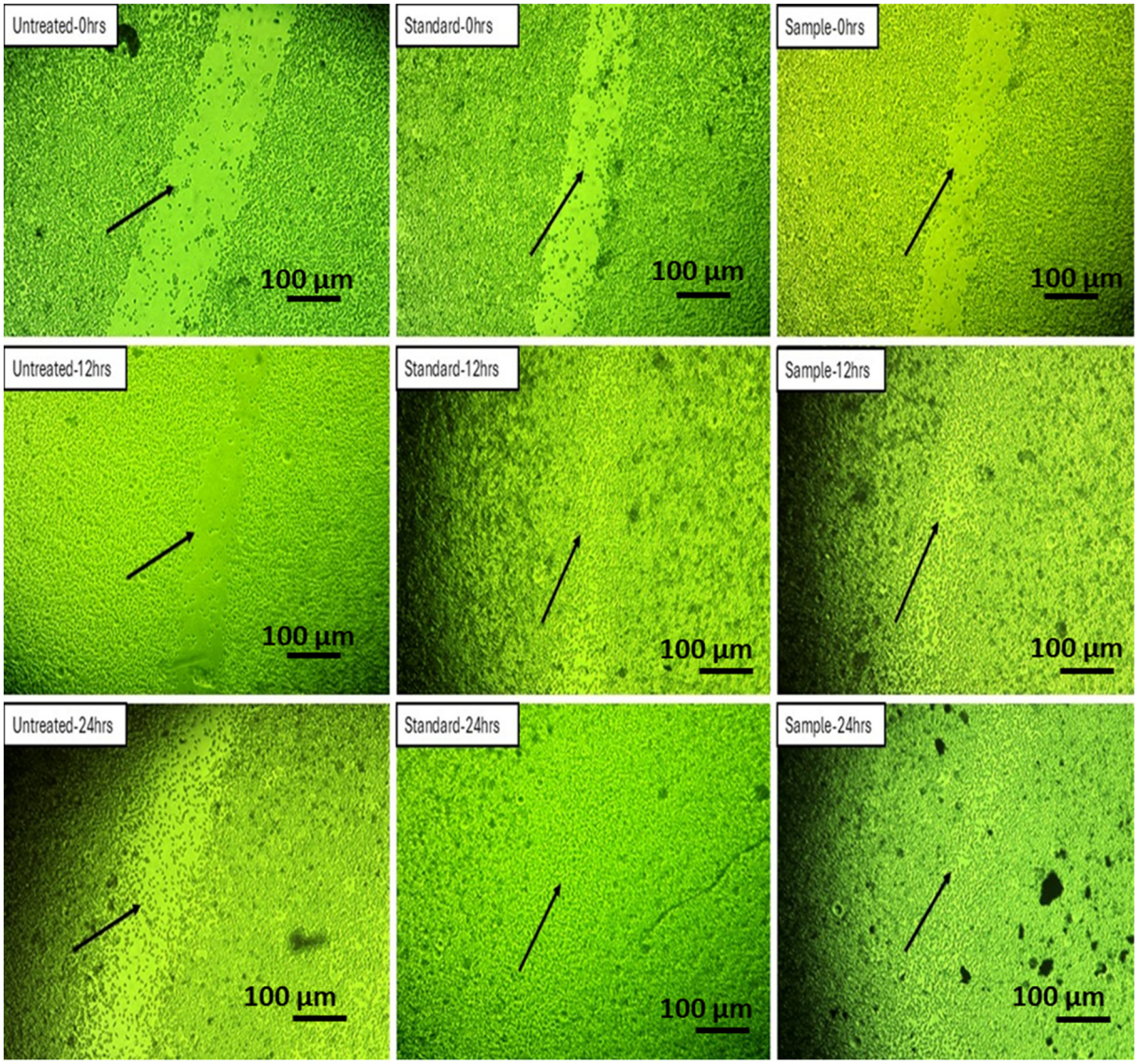

Fig. 13 Wound healing activity of CS-Cu_2O/ZnO NC on L929 cell line using scratch assay.

4. Conclusions

This investigation delineates the fabrication of a phyto-mediated, chitosan-anchored Cu_2O/ZnO nanocomposite (CS-Cu_2O/ZnO NC), synthesized *via* an eco-benign route employing water calyx fluid of *Spathodea campanulata* as a biogenic reducing and stabilizing matrix. Comprehensive physicochemical analyses authenticated the formation of a structurally robust, morphologically uniform, and nanoscale hybrid system. The nanocomposite exhibited superior cisplatin encapsulation efficiency, coupled with a sustained and pH-responsive release kinetics, achieving a cumulative drug release of 94.88% over 72 hours. *In vitro* bioevaluation revealed potent, concentration-dependent cytotoxicity against A375 melanoma cells (IC_{50} = 29.84 µg mL^{-1}), with appreciably reduced cytotoxicity toward L929 fibroblasts, underscoring its selective antineoplastic potential. Additionally, the nano construct demonstrated pronounced regenerative efficacy in scratch wound healing assays, indicative of its favorable cytocompatibility and pro-migratory influence on fibroblast cells. Taken together, these findings position the CS-Cu_2O/ZnO NC as a next-generation, multifunctional theranostic platform, seamlessly integrating targeted drug delivery, oncological intervention, and tissue repair within a sustainable nanotechnological framework. The strategic harnessing of phytochemical constituents for nanomaterial engineering exemplifies a paradigm shift toward greener, more intelligent nanomedicine design, with broad translational implications for precision therapeutics.

Author contributions

Manojna R. Nayak: formal analysis, conceptualization, investigation, data curation, software, methodology, visualization.

Ravindra R. Kamble: supervision, project administration, formal analysis, investigation, resources. Lokesh Bheemayya: visualization, formal analysis, validation. Vishwa B. Nadoni: formal analysis, validation. Amruta Patri: formal analysis, visualization. Mallika Wali: formal analysis, visualization. Arun K Shettar: visualization, data curation, methodology. Joy H Hoskeri: methodology, visualization, data curation. Rangappa S. Keri: data curation, formal analysis, validation. Ashok M. Sajjan: formal analysis, visualization.

Conflicts of interest

The authors declare that they have no known competing financial interests or personal relationships that could have appeared to influence the work reported in this paper.

Ethics approval and consent to participate

There are no human subjects involved in this study. No consent to participate is required.

Data availability

The data that support the findings of this study are available from the corresponding author upon reasonable request.

Supplementary information (SI) is available. Includes anatomy, herbarium voucher, bud collection and WCF extraction, along with UV–Vis, FTIR, and GC–MS analysis of Spathodea campanulata WCF. See DOI: https://doi.org/10.1039/d5pm00392j.

Acknowledgements

The author wishes to express their gratitude to the DST's Sophisticated Analytical Instrumentation Facility (SAIF), and the University Scientific Instrumentation Center (USIC), Karnatak University, Dharwad, India for supplying spectral characterization and the amenities that were necessary to carry out the experiments. CNMS Jain University, Bangalore, India is also acknowledged for providing FESEM data.

References

1 A. Singh and P. K. Dutta, Green synthesis, characterization and biological evaluation of chitin glucan-based zinc oxide nanoparticles and its curcumin conjugation, *Int. J. Biol. Macromol.*, 2020, **156**, 514–521.
2 V. Yadav, S. Banerjee, S. Bairagi, S. Baisoya and S. W. Ali, Green synthesis of sodium lignosulfonate nanoparticles using chitosan for significantly enhanced multifunctional characteristics, *Int. J. Biol. Macromol.*, 2022, **211**, 380–389.
3 A. Ali and S. Ahmed, Green synthesis of metal and metal oxide nanoparticles and their various applications, in *Handbook of Ecomaterials*, 2018, vol. 1, pp. 1–45.
4 S. A. Akintelu, A. S. Folorunso, F. A. Folorunso and A. K. Oyebamiji, Green synthesis of copper oxide nanoparticles for biomedical application and environmental remediation, *Heliyon*, 2020, **6**, e04508.
5 V. V. T. Padil and M. Černík, Green synthesis of copper oxide nanoparticles using gum karaya as a biotemplate and their antibacterial application, *Int. J. Nanomed.*, 2013, **8**, 889–898.
6 Y. A. Selim, M. A. Azb, I. Ragab and M. H. M. Abd El-Azim, Green synthesis of zinc oxide nanoparticles using aqueous extract of *Deverra tortuosa* and their cytotoxic activities, *Sci. Rep.*, 2020, **10**, 3445.
7 B. A. Fahimmunisha, R. Ishwarya, M. S. AlSalhi, S. Devanesan, M. Govindarajan and B. Vaseeharan, Green fabrication, characterization and antibacterial potential of zinc oxide nanoparticles using *Aloe socotrina* leaf extract: a novel drug delivery approach, *J. Drug Delivery Sci. Technol.*, 2020, **55**, 101465.
8 K. Nagpal, S. K. Singh and D. N. Mishra, Chitosan nanoparticles: a promising system in novel drug delivery, *Chem. Pharm. Bull.*, 2010, **58**, 1423–1430.
9 A. Haider, S. Khan, D. N. Iqbal, M. Shrahili, S. Haider, K. Mohammad, A. Mohammad, M. Rizwan, Q. Kanwal and G. Mustafa, Advances in chitosan-based drug delivery systems: a comprehensive review for therapeutic applications, *Eur. Polym. J.*, 2024, **210**, 112983.
10 A. T. Iacob, F. G. Lupascu, M. Apotrosoaei, I. M. Vasincu, R. G. Tauser, D. Lupascu, S. E. Giusca, I. D. Caruntu and L. Profire, Recent biomedical approaches for chitosan-based materials as drug delivery nanocarriers, *Pharmaceutics*, 2021, **13**, 587.
11 N. Duceppe and M. Tabrizian, Advances in using chitosan-based nanoparticles for *in vitro* and in vivo drug and gene delivery, *Expert Opin. Drug Delivery*, 2010, **7**, 1191–1207.
12 L. Meng, W. Huang, D. Wang, X. Huang, X. Zhu and D. Yan, Chitosan-based nanocarriers with pH and light dual response for anticancer drug delivery, *Biomacromolecules*, 2013, **14**, 2601–2610.
13 W. Mushtaq, M. Ishtiaq, M. Maqbool, M. W. Mazhar, R. Casini, A. M. Abd-ElGawad and H. O. Elansary, Green synthesis of zinc oxide nanoparticles using *Viscum album* extracts: unveiling bioactive compounds, antibacterial potential and antioxidant activities, *Plants*, 2023, **12**, 2130.
14 K. Rambabu, G. Bharath, F. Banat and P. L. Show, Green synthesis of zinc oxide nanoparticles using *Phoenix dactylifera* waste as bioreductant for effective dye degradation and antibacterial performance, *J. Hazard. Mater.*, 2021, **402**, 123560.
15 Y. A. Selim, M. A. Azb, I. Ragab and M. H. M. Abd El-Azim, Green synthesis of zinc oxide nanoparticles using aqueous extract of *Deverra tortuosa* and their cytotoxic activities, *Sci. Rep.*, 2020, **10**, 3445.
16 G. K. Padhy, *Spathodea campanulata* P. Beauv.: a review of its ethnomedicinal, phytochemical and pharmacological profile, *J. Appl. Pharm. Sci.*, 2021, **11**, 017–044.

17 A. S. Wagh and S. R. Butle, Plant profile, phytochemistry and pharmacology of *Spathodea campanulata* P. Beauvais: a review, *Int. J. Pharm. Pharm. Sci.*, 2018, **10**, 1–6.
18 S. C. Heim, F. A. Guarnier, D. T. Ferreira, R. Braz-Filho, R. Cecchini and A. L. Cecchini, Antioxidant activity of *Spathodea campanulata* extracts, *Rev. Bras. Plant. Med.*, 2012, **14**, 287–292.
19 F. C. Akharaiyi, B. Boboye and F. C. Adetuyi, Antibacterial, phytochemical and antioxidant activities of leaf extracts of *Gliricidia sepium* and *Spathodea campanulata*, *World Appl. Sci. J.*, 2012, **16**, 523–530.
20 D. Duryat, R. I. Ghozali, Y. J. Saragih, R. Rodiani, T. Maryono, C. Y. Pardilawati and I. Ismanto, Exploration of bioactive compounds in invasive plant *Spathodea campanulata* flower from Bukit Barisan National Park, Indonesia, *Biodiversitas*, 2025, **26**, 1–10.
21 I. A. Gbemisola, J. O. Faluyi and O. Osoniyi, Evaluation of the effect of *Spathodea campanulata* flower bud exudate on cataractogenesis in rat lenses, *Afr. J. Tradit., Complementary Altern. Med.*, 2014, **11**, 83–91.
22 G. A. Govindasamy, R. B. S. M. N. Mydin, N. K. R. Gadaime and S. Sreekantan, Phytochemicals, biodegradation, cytocompatibility and wound healing profiles of chitosan film embedded green synthesized antibacterial ZnO/CuO nanocomposite, *J. Polym. Environ.*, 2023, **31**, 4393–4409.
23 G. A. Govindasamy, R. B. S. M. N. Mydin, W. N. F. W. E. Effendy and S. Sreekantan, Novel dual-ionic ZnO/CuO embedded in porous chitosan biopolymer for wound dressing application: physicochemical, bactericidal, cytocompatibility and wound healing profiles, *Results Chem.*, 2022, **4**, 100386.
24 G. A. Govindasamy, R. B. S. M. N. Mydin, S. Sreekantan and N. H. Harun, Compositions and antimicrobial properties of binary ZnO–CuO nanocomposites encapsulated calcium and carbon from Calotropis gigantea targeted for skin pathogens, *Sci. Rep.*, 2021, **11**, 99.
25 G. A. Govindasamy, R. B. S. M. N. Mydin, S. Sreekantan and N. H. Harun, Effect of calcination temperature on physicochemical and antimicrobial properties of green synthesised ZnO/C/Ca nanocomposites using Calotropis gigantea leaves, *Adv. Nat. Sci.: Nanosci. Nanotechnol.*, 2021, **12**, 015013.
26 G. A. Govindasamy, R. B. S. M. N. Mydin, N. H. Harun, W. N. F. W. E. Efendy and S. Sreekantan, Giant milkweed plant-based copper oxide nanoparticles for wound dressing application: physicochemical, bactericidal and cytocompatibility profiles, *Chem. Pap.*, 2023, **77**, 1181–1200.
27 G. A. Govindasamy, S. Sreekantan, K. A. Saharudin, M. T. Ong, P. J. Thavamany, G. Sahgal and A. A. Tan, Effect of compositions and heat treatments of polypropylene/PP-g-MAH/CuO–TiO_2 composites on thermal, crystallization and antimicrobial properties, *BioNanoScience*, 2024, **14**, 2678–2690.
28 G. A. Govindasamy, S. Sreekantan, K. A. Saharudin, R. Poliah, M. T. Ong, P. J. Thavamany, G. Sahgal and A. A. Tan, Composition-dependent physicochemical and bactericidal properties of dual Cu–TiO_2 nanoparticles incorporated in polypropylene, *BioNanoScience*, 2024, **14**, 770–782.
29 S. A. Aldossary, Review on pharmacology of cisplatin: clinical use, toxicity and mechanism of resistance, *Biomed. Pharmacol. J.*, 2019, **12**, 7–15.
30 N. D. Eljack, H. Y. M. Ma, J. Drucker, C. Shen, T. W. Hambley, E. J. New, T. Friedrich and R. J. Clarke, Mechanisms of cell uptake and toxicity of the anticancer drug cisplatin, *Metallomics*, 2014, **6**, 2126–2133.
31 R. Mezencev, Interactions of cisplatin with non-DNA targets and their influence on anticancer activity and drug toxicity: the complex world of the platinum complex, *Curr. Cancer Drug Targets*, 2014, **14**, 794–816.
32 A. El-Sheikh and Z. Khired, Interactions of analgesics with cisplatin: modulation of anticancer efficacy and potential organ toxicity, *Medicina*, 2021, **58**, 46.
33 K. L. Donaldson, G. L. Goolsby and A. F. Wahl, Cytotoxicity of the anticancer agents cisplatin and taxol during cell proliferation and the cell cycle, *Int. J. Cancer*, 1994, **57**, 847–855.
34 I. Raeisi and Z. Yousefipour, Dual-responsive drug carrier based on zeolitic imidazolate framework-8 incorporated into gold nanoparticles/chitosan/copper sulfide for controlled drug delivery, *J. Drug Delivery Sci. Technol.*, 2024, **98**, 105883.
35 A. Lončarević, S. Clara-Trujillo, A. Martínez-Férriz, M. Blanco-Gómez, G. Gallego-Ferrer and A. Rogina, Chitosan–copper microparticles as doxorubicin microcarriers for bone tumor therapy, *Int. J. Pharm.*, 2024, **659**, 124245.
36 S. Niu, X. Zhang, G. R. Williams, J. Wu, F. Gao, Z. Fu, X. Chen, S. Lu and L. M. Zhu, Hollow mesoporous silica nanoparticles gated by chitosan–copper sulfide composites as theranostic agents for breast cancer treatment, *Acta Biomater.*, 2021, **126**, 408–420.
37 Z. Jin, G. Hu and K. Zhao, Mannose-anchored quaternized chitosan/thiolated carboxymethyl chitosan composite nanoparticles as mucoadhesive drug carriers, *Carbohydr. Polym.*, 2022, **283**, 119174.
38 V. Sihorkar and S. P. Vyas, Potential of polysaccharide-anchored liposomes in drug delivery, targeting and immunization, *J. Pharm. Pharm. Sci.*, 2001, **4**, 138–158.
39 A. O. Adebayo, Y. A. Alli, A. Bamisaye and S. Adewuyi, Nano-chitosan-anchored copper ferrite as a smart magnetic nanocomposite for drug delivery, *Emergent Mater.*, 2024, **7**, 343–351.
40 T. K. Giri, A. Thakur, A. Alexander, H. Badwaik and D. K. Tripathi, Modified chitosan hydrogels as drug delivery and tissue engineering systems: present status and applications, *Acta Pharm. Sin. B*, 2012, **2**, 439–449.
41 H. T. Nguyen, N. H. Do, H. D. Lac, P. L. Nguyen and P. K. Le, Synthesis, properties and applications of chitosan hydrogels as anti-inflammatory drug delivery systems, *J. Porous Mater.*, 2023, **30**, 655–670.
42 C. Wang, F. Li, T. Zhang, M. Yu and Y. Sun, Recent advances in anti-multidrug resistance nano-drug delivery systems, *Drug Delivery*, 2022, **29**, 1684–1697.

43 L. Gao, F. Meng, Z. Yang, M. Lafuente-Merchan, L. M. Fernández, Y. Cao, K. Kusamori, M. Nishikawa, S. Itakura, J. Chen and X. Huang, Nano-drug delivery systems for multidrug-resistant breast cancer: current status and future perspectives, *Biomed. Pharmacother.*, 2024, **179**, 117327.
44 X. Shao, X. Zhao, B. Wang, J. Fan, J. Wang and H. An, Tumor microenvironment-targeted nano-drug delivery systems for multidrug-resistant tumor therapy, *Theranostics*, 2025, **15**, 1689.
45 G. Kibria, H. Hatakeyama and H. Harashima, Cancer multidrug resistance: mechanisms and strategies for circumvention using drug delivery systems, *Arch. Pharmacal Res.*, 2014, **37**, 4–15.
46 I. E. Mba and E. I. Nweze, Nanoparticles as therapeutic options for treating multidrug-resistant bacteria: progress, challenges and prospects, *World J. Microbiol. Biotechnol.*, 2021, **37**, 108.
47 B. Chen, C. Wu, R. X. Zhuo and S. X. Cheng, A self-assembled albumin-based multidrug delivery nanosystem to overcome multidrug resistance, *RSC Adv.*, 2015, **5**, 6807–6814.
48 R. Xing, A. A. Bhirde, S. Wang, X. Sun, G. Liu, Y. Hou and X. Chen, Hollow iron oxide nanoparticles as multidrug-resistant drug delivery and imaging vehicles, *Nano Res.*, 2013, **6**, 1–9.
49 S. Dawar, N. Singh, R. K. Kanwar, R. L. Kennedy, R. N. Veedu, S. F. Zhou, S. Krishnakumar, S. Hazra, S. Sasidharan, W. Duan and J. R. Kanwar, Multifunctional and multitargeted nanoparticles to overcome drug resistance in cancers, *Drug Discov. Today*, 2013, **18**, 1292–1300.
50 X. Wang, Z. Teng, H. Wang, C. Wang, Y. Liu, Y. Tang, J. Wu, J. Sun, H. Wang, J. Wang and G. Lu, Increasing doxorubicin cytotoxicity in multidrug-resistant breast cancer using mesoporous silica nanoparticles, *Int. J. Clin. Exp. Pathol.*, 2014, **7**, 1337–1348.
51 S. M. Sivakumar, Therapeutic potential of chitosan nanoparticles as antibiotic delivery systems for multidrug resistance, *Asian J. Pharm.*, 2016, **10**, 1–6.
52 M. Ye, Y. Han, J. Tang, Y. Piao, X. Liu, Z. Zhou, J. Gao, J. Rao and Y. Shen, Tumor-specific cascade amplification drug release nanoparticles for overcoming multidrug resistance, *Adv. Mater.*, 2017, **29**, 1702342.
53 F. Wang, Y. C. Wang, S. Dou, M. H. Xiong, T. M. Sun and J. Wang, Doxorubicin-tethered responsive gold nanoparticles for overcoming multidrug resistance, *ACS Nano*, 2011, **5**, 3679–3692.
54 S. Rani and T. Ritter, The exosome: a naturally secreted nanoparticle and its application in wound healing, *Adv. Mater.*, 2016, **28**, 5542–5552.
55 S. S. D. Kumar, N. K. Rajendran, N. N. Houreld and H. Abrahamse, Silver nanoparticle and biopolymer-based biomaterials for wound healing, *Int. J. Biol. Macromol.*, 2018, **115**, 165–175.
56 M. Rybka, Ł. Mazurek and M. Konop, Wound dressings containing silver and silver nanoparticles: experimental and clinical perspectives, *Life*, 2022, **13**, 69.
57 N. A. Ismail, K. A. M. Amin, F. A. A. Majid and M. H. Razali, Gellan gum–TiO_2 nanoparticle biofilm as wound dressing material, *Mater. Sci. Eng., C*, 2019, **103**, 109770.
58 A. A. Rakhmetova, T. P. Alekseeva, O. A. Bogoslovskaya, I. O. Leipunskii, I. P. Ol'Khovskaya, A. N. Zhigach and N. N. Glushchenko, Wound-healing properties of copper nanoparticles, *Nanotechnol. Russ.*, 2010, **5**, 271–276.
59 M. Batool, S. Khurshid, Z. Qureshi and W. M. Daoush, Adsorption, antimicrobial and wound-healing activities of biosynthesized zinc oxide nanoparticles, *Chem. Pap.*, 2021, **75**, 893–907.
60 M. Kaushik, R. Niranjan, R. Thangam, B. Madhan, V. Pandiyarasan, C. Ramachandran, D. H. Oh and G. D. Venkatasubbu, Antimicrobial activity and wound-healing potential of ZnO nanoparticles, *Appl. Surf. Sci.*, 2019, **479**, 1169–1177.
61 M. S. Saddik, M. M. Elsayed, M. A. El-Mokhtar, H. Sedky, J. A. Abdel-Aleem, A. M. Abu-Dief, M. F. Al-Hakkani, H. L. Hussein, S. A. Al-Shelkamy, F. Y. Meligy and A. Khames, Azithromycin-loaded zinc oxide nanoparticles for wound healing, *Pharmaceutics*, 2022, **14**, 111.
62 S. Visnuvinayagam, L. N. Murthy, A. Jeyakumari, U. Parvathy, R. Anandan, G. K. Sivaraman and C. N. Ravishankar, Zinc oxide nanoparticle-incorporated chitosan for enhanced wound healing, *J. Environ. Biol.*, 2019, **40**, 691–697.
63 A. Butsyk, Y. Varava, R. Moskalenko, Y. Husak, A. Piddubnyi, A. Denysenko, V. Korniienko, A. Ramanaviciute, R. Banasiuk, M. Pogorielov and A. Ramanavicius, Copper nanoparticle-loaded electrospun patches for infected wound treatment, *Polymers*, 2024, **16**, 2733.
64 P. Sanjarnia, J. Nourmohammadi and S. Hesaraki, Nanocomposite chitosan dressing incorporating polydopamine–copper Janus nanoparticles, *Int. J. Biol. Macromol.*, 2023, **251**, 126173.
65 H. I. Mohamed, N. M. Mahmoud, A. Ramadan, A. M. Al-Subaie, S. B. Ahmed and S. B. Ahmed, Green synthesis of nano-chitosan and copper–chitosan nanocomposites with antibacterial activity, *Nanomaterials*, 2024, **14**, 1111.
66 P. Khosravian, N. Motamedi, M. Javdani and E. M. Khorasgani, Histopathologic evaluation of skin wound healing using chitosan patch with zinc and selenium nanoparticles, *BMC Vet. Res.*, 2025, **21**, 221.
67 L. Sun, J. Han, Z. Liu, S. Wei, X. Su and G. Zhang, Antimicrobial nanoparticle-encapsulated collagenous chitosan matrices for wound repair, *J. Photochem. Photobiol., B*, 2019, **197**, 111539.
68 N. Zisman, N. D. Santos, S. A. Johnstone, A. W. Tsang, D. Bermudes, L. D. Mayer and P. Tardi, Optimizing liposomal cisplatin efficacy through membrane composition manipulation, *Chemother. Res. Pract.*, 2011, **2011**, 1.
69 H. S. Oberoi, N. V. Nukolova, L. Laquer, L. Y. Poluektova, E. Alnouti, Y. Yokohira, A. Arnold, A. V. Kabanov, B. Cohen, G. Bronich and F. Huang, Cisplatin-loaded core cross-

linked micelles: pharmacokinetics and antitumor activity, *Int. J. Nanomed.*, 2012, **7**, 2557–2569.

70 S. Jayakodi and V. Kumar, Green synthesis of CuO nanoparticles and toxicological evaluation, *Biointerface Res. Appl. Chem.*, 2020, **10**, 6343–6353.

71 A. Waris, M. Din, A. Ali, M. Ali, S. Afridi, A. Baset and A. U. Khan, Green synthesis of copper oxide nanoparticles and biomedical applications, *Inorg. Chem. Commun.*, 2020, **123**, 108369.

72 P. K. Pantawane, B. A. Mehere, R. Chahande and A. K. Potbhare, Phytoreduced copper oxide nanoparticles using *Murraya koenigii* leaf extract, *Mater. Today: Proc.*, 2020, **29**, 934–939.

73 M. Asemani and N. Anarjan, Green synthesis of copper oxide nanoparticles using *Juglans regia* leaf extract, *Green Process. Synth.*, 2019, **8**, 557–565.

74 C. Cox, T. N. Teknos, M. N. Barrios, G. J. Brewer, R. D. Dick and S. D. Merajver, Copper suppression as an antiangiogenic strategy in head and neck carcinoma, *Laryngoscope*, 2001, **111**, 696–701.

75 A. Godymchuk, G. A. Frolov, A. Gusev, O. V. Zakharova, E. Yunda, D. Kuznetsov and E. Kolesnikov, Antibacterial properties of copper nanoparticle dispersions, *IOP Conf. Ser.:Mater. Sci. Eng.*, 2015, **98**, 012033.

76 N. Malhotra, T.-R. Ger, B. Uapipatanakul, J. Huang, K. H.-C. Chen and C. Hsiao, Toxicity of copper and copper nanoparticles in fish, *Nanomaterials*, 2020, **10**, 1126.

77 C. Zhang, Y. Fu, X. Zhang, C. Yu, Y. Zhao and S. Sun, BSA-directed synthesis of CuS nanoparticles for photothermal tumor ablation, *Dalton Trans.*, 2015, **44**, 13112–13119.

78 J. Wang and C. Zhang, $CuGeO_3$ nanoparticles as photothermal theranostic agents for cancer therapy, *Front. Bioeng. Biotechnol.*, 2020, **8**, 590518.

79 A. F. Oussou-Azo, T. Nakama, M. Nakamura, T. Futagami and M. C. Vestergaard, Antifungal potential of nanostructured copper and copper oxides, *Nanomaterials*, 2020, **10**, 1003.